CR 137784

BOLT BERANEK AND NEWMAN INC

CONSULTING · DEVELOPMENT · RESEARCH

BBN Report No. 2955

Contract No. NAS2-8382

A STUDY OF NOISE SOURCE LOCATION ON A MODEL SCALE AUGMENTOR WING USING CORRELATION TECHNIQUES

John F. Wilby
Terry D. Scharton

10 November 1975

Submitted to:

National Aeronautics and Space Administration
Ames Research Center
Moffett Field, California 94035

CR-137784

BBN Report No. 2955 Contract No. NAS2-8382

A STUDY OF NOISE SOURCE LOCATION ON A MODEL SCALE AUGMENTOR WING USING CORRELATION TECHNIQUES

John F. Wilby
Terry D. Scharton

10 November 1975

Submitted to:

National Aeronautics and Space Administration
Ames Research Center
Moffett Field, California 94035

SUMMARY

An experimental investigation has been conducted on a model-scale augmentor wing to identify the sources of far-field noise. The measurement procedure followed in the investigation involved the cross-correlation of far field sound pressures with fluctuating pressures on the surface of the augmentor flap and shroud. In addition pressures on the surfaces of the augmentor were cross-correlated. The results are interpreted as showing that the surface pressure fluctuations are mainly aerodynamic in character and are convected in the downstream direction with a velocity which is dependent on the jet exhaust velocity. However the far field sound levels in the mid and high frequency ranges are dominated by jet noise. There is an indication that in the low frequency range trailing edge noise, associated with interaction of the jet flow and the flap trailing edge, plays a significant role in the radiated sound field.

The test program in the NASA Ames 7'x10' Wind Tunnel was coordinated by the Technical Monitor, Mr. Michael D. Falarski, and the authors wish to acknowledge his helpful support in the measurement program.

TABLE OF CONTENTS

1. INTRODUCTION

Several propulsive lift systems are being considered as a means of providing short take-off and landing (STOL) capabilities for commercial airplanes. One such lift system is the augmentor wing, in which high speed gas flow is discharged from nozzles at the wing trailing edge, into an ejector formed by the wing flap and shroud. In common with other propulsive lift systems, the augmentor wing generates noise. However some noise reduction can be achieved by placing sound absorbing material on the flap and shroud surfaces which are adjacent to the flow from the nozzle. This technique has been demonstrated experimentally, on model scale systems [1], for mid-frequency ranges but the effectiveness of the lining decreases at high and low frequencies.

As part of a program to improve the noise reduction characteristics of the augmentor wing, NASA Ames Large Scale Aerodynamics Branch initiated an investigation to determine the locations of noise sources of the augmentor system. With this information, augmentor wing design can be optimized for minimum far field noise. Within this investigation, Bolt Beranek and Newman (BBN) had the role of providing research assistance in the planning, performance and analysis of model scale acoustic tests in the NASA Ames #1 7'x10' wind tunnel. This report contains BBN's analysis of the test data, particular emphasis being placed on the pressure correlation measurements. Pressure correlation coefficients are considered for surface-far field transducer pairs and for surface-surface pairs. The relationship between pressures on the surface of the flap or shroud and the acoustic pressures in the far field can be related to noise source location. Measurements relating

surface pressures at two different locations on the flap or shroud can be used in determining the characteristics of the surface pressure field with respect to noise generation.

In this report, Section 2 presents a brief outline of correlation techniques as applied to the two areas identified above. The outline provides the basis for subsequent analysis of the test data. Section 3 describes the test program, and characteristics of the fluctuating pressure field on the surfaces of the flap and shroud are presented in Section 4. Correlations between surface pressures on the flap or shroud and acoustic pressures in the far field are analyzed in Section 5. The data are interpreted in terms of noise source location and noise generation. Then, in Section 6, the effect of free stream flow speed is introduced. Section 7 discusses the experimental results and Section 8 presents conclusions and recommendations based on BBN's analysis of the experimental results.

2. PRESSURE CORRELATION COEFFICIENTS

In this section pressure correlation coefficients relating surface pressures to the acoustic far field are described under a series of simplifying assumptions. It is shown that the correlation coefficient can be used as an estimate of the number of independent noise sources located at the region of highest correlation. The analysis assumes that the far field acoustic pressures result from the conversion from aerodynamic to acoustic pressures at the flap and shroud surfaces, with subsequent propagation to the far field as acoustic waves. However it has to be borne in mind that acoustic pressures can be present within the augmentor and that the surface transducers are sensitive to vibration as well as pressure signals.

Spectral and correlation information for the surface pressures can be used in several ways to describe the characteristics of the pressure field of an augmentor wing. The data can, in turn, be interpreted in terms of noise sources. In particular, the data from the present tests have been analyzed to determine effective length scales in the pressure field and to identify the presence of acoustic and vibration components.

2.1 Surface and Far Field Correlations

The surface-far field correlation coefficient is obtained by measuring the fluctuating pressure $p_s(t)$ on the surface of the flap and the acoustic pressure $p_a(t)$ in the far field. The resulting correlation coefficient is defined as

$$\rho_{s,a}(\tau) = \frac{\langle p_s(t)p_a(t+\tau)\rangle}{\sqrt{\langle p_s^2(t)\rangle\langle p_a^2(t)\rangle}} \qquad (1)$$

where the symbols <> indicate time averages, and τ is the time delay. Equation (1) indicates that the rms pressures on the surface and in the far field are used as normalizing parameters.

It is now possible, with simplifying assumptions, to relate $\rho_{s,a}(\tau)$ to the acoustic energy radiated by the surface of the flap or shroud in the neighborhood of the measuring transducer.

First, assume that $p_s(t)$ is purely aerodynamic. Then the associated acoustic pressure in the far field at distance R and angle θ is [2]

$$p(R,t) = \frac{-\cos\theta}{4\pi c}\frac{1}{R}\int_S \frac{\partial}{\partial t} p_s(S,t-R/c)dS \qquad (2)$$

Next, assume that the far field pressure is the sum of the contributions from N independent surface pressures p_s^i with associated areas S^i

$$\text{i.e.} \qquad \langle p_s^i p_s^j \rangle = \delta_{ij}(p_s^i)^2 \qquad (3)$$

Then, for band-limited signals, centered at angular frequency ω, equation (2) can be rewritten in the form

$$p(R,\omega) = \sum_{i=1}^{N} p_s^i(\omega) s^i(R,\omega) \qquad (4)$$

where

$$s^i(R,\omega) = \frac{\sqrt{-1}\ \omega \cos\theta\ S^i}{4\pi c R} \qquad (5)$$

Here, $s^i(R,\omega)$ represents the conversion from aerodynamic to acoustic pressure.

It can be shown now that the square of the correlation coefficient $\rho_{s,a}(\tau)$, evaluated at $\tau = \tau_m$ where τ_m is the time delay for

maximum correlation, is a measure of the mean square acoustic pressure at R, which is contributed by area S^i. From equation (1)

$$\rho^2_{s,a}(\tau_m) = \frac{\langle p^i_s(t) p_a(t+\tau_m)\rangle^2}{\langle p^{i2}_s(t)\rangle\langle p^2_a(t)\rangle}$$

But, from equation (4)

$$p_a(t+\tau_m) = \sum p^i_s(t) s^i(\omega)$$

Hence, using equation (3),

$$\langle p^i_s(t) p_a(t+\tau_m)\rangle = \langle p^{i2}_s(t)\rangle s^i(\omega)$$

and equation (6) reduces to

$$\rho_{s,a}{}^2(\tau_m) = \frac{\langle p^{i2}_s(t)\ s^{i2}(\omega)}{\langle p^2_a(t)\rangle} \qquad (7)$$

Thus the square of the correlation coefficient gives the mean square acoustic pressure contributed by area S^i, as a fraction of the total mean square acoustic pressure at R.

Assuming that all N noise sources contribute equally to the radiated sound, then

$$N = \frac{1}{\rho^2_{s,a}(\tau_m)} \qquad (8)$$

The preceding discussion is in general terms, but the form of the correlation coefficient can be expressed in more detail. In practice the surface and far field pressure spectra are broadband and the spectrum level changes slowly with frequency. Thus, within an octave band, the spectrum level can be taken as constant. Further, acoustic waves are non-dispersive. The correlation coefficient can now be written in the form [3]

$$\rho_{s,a}(\tau) = \rho_{s,a}(\tau_m) \cdot \frac{\sin \pi B(\tau-\tau_m)}{\pi B(\tau-\tau_m)} \cdot \cos 2\pi f(\tau-\tau_m) \qquad (9)$$

where B is the filter bandwidth in Hertz and f is the filter center frequency (Hz). Neglecting any effects of the jet flow, the value of τ_m is the time taken for sound waves to propagate from the surface location to the far field

$$\text{i.e.} \quad \tau_m = \frac{R}{c} \qquad (10)$$

Equation (9) indicates that the correlation coefficient is a cosine function which decays in a $\frac{\sin x}{x}$ manner. Thus the maximum value of the correlation coefficient occurs when the modulating function $\sin \frac{\pi B(\tau-\tau_m)}{\pi B(\tau-\tau_m)}$ is unity.

If several propagation paths are present, such as is the case for the direct signal and signals reflected from the walls of the test section, the correlation coefficient becomes

$$\rho_{s,a}(\tau) = \sum_{j=1}^{n} \rho^{j}_{s,a}(\tau_j) \frac{\sin \pi B(\tau-\tau_j)}{\pi B(\tau-\tau_j)} \cos 2\pi f(\tau-\tau_j) \qquad (11)$$

The coefficient has a series of maxima at τ_j, with value $\rho^{j}_{s,a}(\tau_j)$. Also the correlation maximum associated with the direct signal will be lower than the value measured in the absence of reflected signals. For example, consider the simple case of the direct and one reflected signal. The measured correlation coefficient is

$$\rho_{s,a}(\tau) = \frac{\rho^{1}_{s,a}(\tau)}{\sqrt{2-\alpha}} + \sqrt{\frac{1-\alpha}{2-\alpha}}\, \rho^{1}_{s,a}(\tau-t') \qquad (12)$$

where $\rho^{1}_{s,a}(\tau)$ is the correlation coefficient in an anechoic space and α is the reflection coefficient. Equation (12) assumes that the signal is sufficiently broadband that

$$\langle p^1_{s,a}(t) p^1_{s,a}(t-t') \rangle \simeq 0 \quad .$$

It is seen that the correlation coefficient for the direct signal is reduced by the factor $\frac{1}{\sqrt{2-\alpha}}$.

2.2 Surface Correlations

Within the augmentor, the flow can be considered to be two-dimensional, with turbulence being convected in the chordwise direction. Airflow discharged from the nozzle will become attached to the upper surface of the flap, but may not become attached to the shroud.

Correlation measurements in flow conditions of the above type have been conducted by several investigators, and the results can be applied to the present analysis. For example, Bull [4] has studied the pressure fluctuations on the wall beneath a turbulent boundary layer, and Maestrello et al [5] have made measurements in the near field of a model scale air jet. In both cases it was assumed that the correlation coefficient for the surface pressures decayed exponentially in the spatial domain, a relationships which was in agreement with the experimental data.

For near field jet noise Maestrello et al [5] represented the broadband pressure correlation coefficient by

$$\rho(\xi_1, \xi_3, \tau) = e^{-\gamma_1 |\xi_1|} e^{-\alpha_3 |\xi_3|} e^{-\gamma_2 |\tau|} \cos(2\pi f_o \tau - k_o \xi_1) \qquad (13)$$

where separation distances ξ_1, ξ_3 are respectively parallel and perpendicular to the flow, f_o is a characteristic frequency,

and $k_o = 2\pi f_o/U_c$ where U_c is the mean convection velocity of the pressure field. The data show

$$U_c \simeq 0.65\ U_j$$

where U_j is the jet exit velocity.

Bull described the boundary layer pressure field in terms of the narrowband correlation coefficient

$$\rho(\xi_1,\xi_3,\tau;f,B) = A(B,\tau)e^{-\beta_1|\xi_1|}e^{-\beta_3|\xi_3|}\cos(2\pi ft-k\xi_1) \qquad (14)$$

where $A(B,\tau)$ is a function depending on the characteristics of the frequency filter with bandwidth B and center frequency f, and wavenumber $k = \omega/U_c(\omega)$. Equation (14) is similar in form to that developed by White [3] for a dispersive system of waves. Then

$$A(B,\tau) = \frac{\sin \pi B(\tau-\xi_1/U_g)}{\pi B(\tau-\xi_1/U_g)} \qquad (15)$$

where U_g is the group velocity for the pressure field, and $U_c(\omega)$, above, is the phase velocity. Data from Bull [4] show phase velocities in the range $0.6U_\infty$ to $0.9U_\infty$ where U_∞ is the free stream velocity.

A lateral length scale for the surface pressure field can be defined by

$$\Lambda_3 = 2\int_0^\infty |\rho(0,\xi_3,0;f,B)|\,d\xi_3$$

$$= \frac{2}{\beta_3} \qquad \text{from equation (14)} \qquad (16)$$

A characteristic length scale in the longitudinal (or flow) direction, is

$$\Lambda_1 = 2\int_0^\infty |\rho(\xi_1,0,\xi_1/U_g;f,B)|\,d\xi_1$$

$$= \frac{2}{\beta_1} \qquad (17)$$

although in this case Λ_1 is not a length scale in the true sense. Rather, it represents the time scale T_1 for which pressures are correlated in a moving frame of reference:

$$T_1 = \frac{\Lambda_1}{U_g} \qquad (18)$$

The above simplified analysis assumes implicitly that the signals measured by the surface transducers are due solely to the action of local aerodynamic pressures on the sensitive element of the transducer. This may not be the case in practice. There may be an acoustic pressure field within the augmentor, or transducer vibration may introduce an additional signal component. In either case the surface-surface pressure correlation coefficient will be modified.

There are several possibilities, including:

(a) Additional signals uncorrelated with the aerodynamic pressures and with each other. Then the measured correlation coefficient will have a value which is lower than the ideal case, by the factor

$$\frac{p_{rms}(\text{aerodynamic alone})}{p_{rms}(\text{aerodynamic + other})}$$

(b) Additional signals uncorrelated with aerodynamic pressures but correlated with each other at time delays which are different from those for the aerodynamic pressure field.

Then there will be additional maxima in the correlation coefficient, and the measured value of the coefficient associated with the aerodynamic field will be lower than the ideal value, as in (a).

(c) Conditions as in (b), except that all signal components have maximum correlation at the same time delay. The net effect on the measured value of the correlation coefficient is difficult to predict.

3. WIND TUNNEL TESTS

The measurements discussed in this report were made in the NASA Ames #1 7'x10' wind tunnel. The surfaces of the tunnel test section were covered with a 8.6 cm (3-inch) layer of Scottfelt to reduce the acoustic reverberation and a model scale augmentor wing was mounted on the tunnel centerline (Figure 1). The propulsion nozzle of the model had 43 lobes with width of about 0.25 cm (0.11 inch) and height 2.8 cm (1.1 inch). Model span was 76.2 cm (30 inches).

Surface pressure fluctuations were measured using flush-mounted BBN piezo-electric transducers with 0.25 cm (0.1 inch) diameter sensitive elements. Transducer locations on the flap and shroud are shown in Figure 2. Ten transducers were used; holes without transducers were plugged with modelling clay. The transducers were held in place by modelling clay and some adjustments were necessary, particularly near the trailing edges of the flap and shroud, to minimize the contributions from transducer vibration. The adjustments were made somewhat arbitrarily, using the spectrum shape of the transducer signal as a guideline. It was not possible, within the limitations of the test program, to separate vibration and pressure components.

Far field acoustic pressures were measured using five B and K 1/4 inch microphones with nose cones. The microphones were located on a radius of about 107 cm (42 inches) centered at the nozzle exit, with their axes parallel to the tunnel centerline. Angular locations of the microphones are shown in Figure 3. Polar plots of the acoustic far field were obtained by means of a B and K 1/8 inch microphone on a rotating boom (Figure 1) centered at the nozzle exit plane.

Spectral measurements of the surface and far field pressures were made in one-third octave bands with center frequencies in the range 100-80,000 Hz, using a General Radio Type 1926 Multichannel RMS Detector. The augmentor wing was operated at nozzle plenum pressures of 27.6, 55.2, 82.8, 110.4, 138.0 and 165.6 kN/m^2 (4,8,12,16,20 and 24 psig), i.e. at pressure ratios p_T/p_a of 1.27, 1.54, 1.81, 2.09, 2.36 and 2.63.

Pressure correlation measurements were made between pairs of surface pressure transducers, or between surface transducers and far field microphones. Before correlation, the signals were filtered using similar octave band filters of two B and K sound level meters. Correlations were performed on a Saicor SAI-43A correlator in the clipped mode of operation. The correlation operation was repeated up to three times to magnify the correlation coefficient where necessary. The true value of the correlation coefficient was obtained from the relationship

$$\rho_{true} = \sin\left(\frac{\pi}{2}\,\rho_{clipped}\right)$$

Correlations were obtained in octave bands centered at 0.5, 1, 2, 4, 8 and 16 kHz, for a nozzle pressure ratio of 2.09. This pressure ratio was selected since it gave a high exhaust velocity typical of normal operation, but had no significant discrete frequency shock noise.

4. PRESSURE FIELD ON FLAP AND SHROUD

4.1 Spectra

Pressure spectra measured on the flap and shroud (in the absence of transducer vibration) are broadband in character, with a broad spectral peak. The frequency of this peak increases as nozzle jet velocity increases, and decreases as distance from nozzle exit plane increases.

At a given location on the flap or shroud, the spectra can be collapsed onto a single curve if the frequency is non-dimensionalized with respect to nozzle height h and jet velocity U_j, and the one-third octave band level is normalized with respect to the overall sound pressure level (OASPL). This is shown in Figure 4 for location 11 at the center of the flap, and in Figure 5 for location 40 at the trailing edge of the shroud. The spectra are associated with nozzle pressure ratios of 2.09 and below, where discrete frequency shock noise is not dominant.

Normalization with respect to chordwise location is more complicated. Maestrello et al [5] have shown that, for the pressure spectra in the near field of a three-dimensional jet, the Strouhal number can be modified by a factor $\left[\frac{x}{x_o} + 1\right]^3$ where x is the distance downstream of the nozzle exit plane and $x_o = 5D_j$, where D_j is the jet diameter. In the present case, if D_j is replaced by the nozzle height h, it is found that the exponent 3 has to be replaced by the lower value of 1.5 for the flap (Figure 6), and the higher value of 4 for the shroud. The choice of $x_o = 5h$ as the reference distance is somewhat arbitrary and other functions might give more universal data collapse.

4.2 Correlation Coefficients

Pressure correlation coefficients were determined from measurements along chordwise and spanwise directions. The chordwise measurements were used to determine convection velocities in an attempt to identify acoustic and aerodynamic components. In addition the decay of the correlation coefficient was measured to obtain an estimate of the moving frame length or time scale of the pressure field. Correlation measurements in the spanwise direction were used to obtain lateral length scales for the pressure field. All the correlation measurements were made at a nozzle pressure ratio of 2.09.

Typical correlation coefficients in octave frequency bands are shown in Figure 7 for a separation distance of 2.54 cm (1 inch) in the chordwise direction. The reference transducer was at location 1, near the flap leading edge (in the region of the flow attachment point). The data show a sinusoidal oscillation at the frequency equal to the center frequency of the respective octave band. The cosine function is modulated by a term similar to the $\frac{\sin \pi B(\tau-\xi_1/U_g)}{\pi B(\tau-\xi_1/U_g)}$ term in equations (14) and (15) Thus the measured correlation coefficients can be used to determine the group convection velocity U_g, by taking the time delay associated with the maximum of the envelope to the cosine function.

For octave band center frequencies 2k, 4k and 8kHz, the group convection velocity in the downstream direction is found to be 204 m/s (670 ft/sec) on the flap and 134 m/s (440 ft/sec) on the shroud. Within the accuracy of the experiment these velocities are independent of frequency. On the shroud the convection velocity of 134 m/s was observed also at 1 kHz, but no downstream convection was observed at 1kHz on the flap.

In addition to the downstream convection, there was evidence on the flap of pressure components being convected upstream with velocities in the range 58-73 m/s (190-240 ft/sec). This occurred mainly at 2k and 4kHz and at large separation distances when correlation coefficients for the downstream propagating components were very low. It is possible that the upstream propagation was not observed at small separation distances because of the scale on which the correlations were plotted.

Surface correlation data were found to have no consistent trend at 500 Hz, for reasons which have not yet been identified.

Measured convection speeds for the surface pressures can be compared with values predicted for jet and boundary layer fluctuating pressures. Unfortunately the comparison can be only crude since no detailed measurements were made of the flow velocities within the augmentor. It is known, however, that there is a large velocity gradient across the height of the augmentor. For example, at the augmentor exit the velocity at the flap surface is approximately 145 m/s (475 ft/sec) whereas that at the shroud is only 31 m/s (100 ft/sec).

Results of Maestrello et al [5] for a jet near-field, and Fuchs [10] for a jet mixing region, show a pressure convection velocity of 0.65 V_j. In the present configuration, assuming that the jet total temperature is equal to the ambient temperature, the jet velocity for a nozzle pressure ratio of 2.09 is 332 m/s (1090 ft/sec). The predicted convection velocity is then 216 m/s (708 ft/sec). From Bull's data for a turbulent boundary layer the convection velocity lies in the range 0.6 V_o to 0.8 V_o, where V_o is the local free stream velocity. Taking a mean value of 0.7 V_o, the predicted convection velocity is 232 m/s (760 ft/sec) at the

nozzle and 101 m/s (330 ft/sec) at the flap trailing edge. These predicted velocities are in general agreement with the convection velocity of 204 m/s measured on the flap, but the values are generally higher than the velocity measured on the shroud.

Now, considering the component propagating upstream, the assumption is made that the pressure field is acoustic. The mean flow velocity (average of jet velocity and velocity at flap trailing edge) is 238 m/s (780 ft/sec), and the speed of sound in the jet is 308 m/s (1010 ft/sec). Thus the average upstream velocity of propagation is 70 m/s (230 ft/sec), which is close to the measured value.

Decay of the correlation coefficient in a moving frame of reference in the chordwise direction is shown in Figures 8 and 9 for flap and shroud respectively. The data refer to the peak correlation at optimum time delay τ_m. An exponentially decaying curve has been fitted to each set of data, and the corresponding length (or time) scale (Table I) calculated according to equations (17) and (18).

Table I

Pressure Correlation Scales in Chordwise Direction

Frequency (Hz)	Flap			Shroud		
	Λ_1 (cm)	Λ_1 (inch)	T_1 (ms)	Λ_1 (cm)	Λ_1 (inch)	T_1 (ms)
500	4.3	1.7	-	25.4	10.0	-
1,000	3.6	1.4	0.17	11.9	4.7	0.89
2,000	5.3	2.1	0.26	9.1	3.6	0.68
4,000	6.1	2.4	0.30	6.1	2.4	0.46
8,000	5.8	2.3	0.29	4.6	1.8	0.34

Spanwise pressure correlation measurements were made at three separation distances on the flap leading edge, two separation distances on the flap trailing edge, and one separation distance on shroud leading and trailing edges. The resulting values of the correlation coefficient $\rho\ (o,\xi_3,0,f)$ are shown in Figures 10 and 11.

Reliable estimation of the lateral, or spanwise, correlation length scales is more difficult than for the chordwise direction because correlation coefficients were measured for only a few separation distances. Thus the values of the length scales in Table II should be regarded as tentative.

Table II

Pressure Correlation Length Scales in Spanwise Direction

Frequency	Flap Leading Edge Λ_3		Flap Trailing Edge Λ_3	
(Hz)	(cm)	(inch)	(cm)	(inch)
500	1.30	0.51	-	-
1,000	0.97	0.38	-	-
2,000	0.99	0.39	3.12	1.23
4,000	1.19	0.47	3.53	1.39
8,000	0.97	0.38	2.67	1.05
16,000	0.81	0.32	-	-

Values for Λ_3 on the shroud have not been calculated since measurements were made at only one separation distance. However based on these data the length scales appear to be larger than the corresponding values on the flap, particularly at the leading edge. Figures 10 and 11 indicate that the length scales on the shroud do not increase when moving from leading edge to trailing edge, as they do on the flap (Table II).

5. ACOUSTIC FAR FIELD PRESSURES

5.1 Acoustic Spectra

The radiated sound field was measured at the five fixed locations shown in Figure 3, and polar plots were obtained using a microphone mounted on a boom above the model wing. Spectra were measured at several nozzle pressure ratios, but correlation between surface and far field pressures was measured at only one nozzle pressure ratio, 2.09 (plenum pressure of 110.4 kN/m^2 or 16 psig).

Polar plots were obtained using octave band filters and a typical set of curves is shown in Figure 12. The figure shows that high sound levels occur at angles of approximately 145° and 215° to the jet axis (where 0° is taken as the upstream direction). Below the wing, microphone location 5 is close to the peak at 145°. Thus the location was selected for correlation measurements. Locations 3 and 6, which are respectively at about 90° and 270° to the jet axis, were also selected for correlation measurements. One-third octave band sound pressure spectra measured at these three locations (3, 5 and 6) are shown in Figure 13 for a nozzle pressure ratio of 2.09 and zero tunnel flow.

5.2 Correlation Coefficients

Under ideal circumstances, the correlation coefficient relating surface and far field pressures would show one maximum, at a time delay equal to the propagation time. However in practice other maxima may occur due to reflections and contributions from noise sources located away from the surface transducer. Thus, in the data analysis, the propagation time was estimated for each pair of transducers. It was then assumed that the correlation maximum which occurred at the time delay closest

to the estimated propagation time was that associated with the direct path. Figure 14 shows the agreement between estimated and observed time delays associated with microphones 3, 5 and 6, and transducers close to the flap or shroud leading and trailing edges. The estimated values do not take into account refraction and other effects associated with acoustic propagation in the jet flow, a fact which may account for some of the discrepancies between estimated and measured values.

Some comment is probably appropriate regarding the influence of other correlation maxima on the value of the coefficient for the direct-path signal. The correlation coefficients alone do not provide sufficient information to determine the effects. For example, if two correlation maxima, associated with two uncorrelated noise sources, are of equal magnitude it does not follow that the mean square values of the two signals will be equal. However if appropriate assumptions can be made, some interpretation of the data is possible.

The effect of a single reflected wave is shown in equation (12). Assuming an absorption coefficient of 0.85 for the lining on the test section surface, equation (12) indicates that the correlation coefficient for the direct wave will be reduced by about 7% and the value of the coefficient for the reflected signal will be about 39% of that for the direct wave. Increasing the number of reflected signals will reduce still further the value of the correlation coefficient for the direct signal but will not affect the relative magnitudes of direct and reflected signals. As an example, if there are three reflected waves of equal magnitude, the correlation coefficient associated with the direct wave will be reduced by 17%.

In the present analysis no corrections have been applied to the correlation coefficients to account for the presence of reflected or other signals.

Correlation coefficient maxima relating flap surface pressures and far field acoustic pressures at microphones 3 and 5 are shown in Figures 15 and 16. Similar data for the shroud and microphones 3, 5 and 6 are shown in Figures 17-19. In cases where measurements were made at several spanwise locations, the values of the coefficient have been averaged before being plotted in the figures.

Data associated with the leading and trailing edges of the flap and shroud are plotted in Figures 20 and 21, respectively, as a function of frequency. Figure 20 also contains data for transducer location 13 which is shown in Figures 15 and 16 to be the location of highest correlation on the flap.

Polar distribution of the correlation coefficient maximum is shown in Figure 22 for location 14 on the flap. (A limited amount of data is also presented for location 13.)

The correlation data presented in Figures 15 through 22 refer to measurements in octave bands centered at 500, 1000, 2000, 4000 and 8000 Hz. Correlation coefficients were measured at 16,000 Hz but no significant correlation was observed. Thus data at frequencies above 8000 Hz are not presented in the figures.

6. EFFECT OF FREE STREAM FLOW

For zero tunnel flow tests, the augmentor wing was positioned so that the exhaust flow was parallel to the tunnel centerline. As a consequence the wing had an angle of incidence α of -30°. However this large negative angle was unacceptable for non-zero tunnel flow, and the wing was rotated to an angle of attack closer to zero. The exhaust flow then impinged on the tunnel wall at the downstream edge of the porous lining. Under this new configuration, far field noise measurements were made at microphone locations 2 and 4, instead of 3 and 5. The change in microphone locations meant that the measurements were made at approximately the same angles to the exhaust flow as was the case for the α = -30° tests.

Surface and far field acoustic pressure spectra were measured at three free stream dynamic pressures, 479, 958 and 1437 N/m^2 (10,20 and 30 lb/ft^2), and a nozzle pressure ratio of 2.09. Correlation coefficients for surface and far field pressures were measured at a dynamic pressure of 1437 N/m^2 (30 lb/ft^2).

No large changes were observed in far field sound levels when tunnel flow was introduced. Figure 23 shows typical results for microphone location 4 and tunnel dynamic pressures of 0 and 1437 N/m^2.

Although the particular data in Figure 23 indicate that the presence of tunnel flow increased low frequency sound levels and decreased high frequency levels, data for all three measuring locations (microphones 2, 4 and 6) showed no consistent trend except at frequencies below 400 Hz. At these low frequencies measured sound levels increased when flow was present, but the increase was more likely due to tunnel noise problems than to changes in noise from the augmentor.

For a jet without an augmentor wing system, the radiated sound levels would be expected to decrease as relative jet velocity decreased. Stone [7] accounts for forward motion by replacing jet velocity U_j with $U_j(1 - \frac{U_a}{U_j})^{0.75}$, where U_a is the forward speed of the airplane (in this case the tunnel airspeed). On the basis of a U_j^8 law, the expected reduction in radiation acoustic power would be 4 dB when tunnel dynamic pressure is increased to 1437 N/m^2 (30 lb/ft^2), but this change is not observed in the experimental data.

In contrast to the acoustic far field, low frequency surface pressure levels measured near the flap and shroud trailing edges decrease by an average of 4 dB when tunnel flow is introduced (Figures 24 and 25). However this decrease is not observed at leading edge locations. In fact, at location 25 on the flap, a location which is out of the nozzle exhaust flow, the low frequency pressure fluctuations increase when tunnel flow is present (Figure 26)

The effect of tunnel flow on the surface-far field pressure correlation coefficients is shown in Table III. The data are presented in terms of the ratio of correlation coefficients for test conditions with and without tunnel flow. For the flap measurements, leading edge ratios were obtained by averaging results for locations 6 and 8, and trailing edge ratios are given by average values for locations 13 and 14.

Table III

Ratio of Correlation Coefficients* With and Without Tunnel Flow

Frequency (Hz)		500	1000	2000	4000	8000
Far Field Microphone	Surface Location	$[\rho_{30}(\tau_m)/\rho_o(\tau_m)]$*				
2	Flap leading edge	0.52	0.64	0.91	0.94	1.09
2	Flap trailing edge	0.88	0.48	1.05	0.67	0.92
4	Flap leading edge	0.42	0.84	0.72	1.39	0.92
4	Flap trailing edge	0.39	1.02	0.91	1.91	0.74
4	Shroud trailing edge	0.46	0.91	1.06	1.37	0.69
6	Shroud leading edge	0.84	1.18	0.80	0.65	1.16
6	Shroud trailing edge	0.61	1.61	1.22	-	0.73

*$\rho_o(\tau_m)$ is maximum value of surface-far field correlation coefficient when there is zero tunnel flow. $\rho_{30}(\tau_m)$ is the corresponding value when the tunnel flow has a dynamic pressure of 1437 N/m^2 (30 lb/ft^2).

The data from Table III have been averaged for leading and trailing edges, and the resulting spectra are plotted in Figure 27. For the flap leading and trailing edges the average value of the ratio of correlation coefficients increases, with frequency, from a value of less than unity. This variation indicates that the surface-to-far-field pressure correlation coefficients decrease at low frequencies, but remain unaltered (or perhaps increase) at high frequencies, when tunnel flow is introduced. Data for the shroud trailing edge tend to show a greater increase in correlation coefficient when flow is introduced.

If the ratio of correlation coefficients is averaged over all frequencies and locations in Table III, the average value is 0.90. Restricting the averaging procedure to frequencies in the range 1000-8000 Hz gives an average ratio of 0.98.

Use of an averaging process may be criticized because some of the detailed variations are hidden. However it is possible that some of these variations are really due to experimental scatter and the average trend is more meaningful, particularly that shown in Figure 27.

7. DISCUSSION

Several observations can be made regarding the surface-far field correlation coefficients. These can be summarized as follows:

(a) For most cases the highest correlation between flap and far field occurs near to, but not at, the flap trailing edge.

(b) Flap-far field correlation is higher with respect to microphone 5 than microphone 3, except at 500 Hz.

(c) Highest correlation between shroud and far field usually occurs at the leading edge.

(d) Highest correlation for flap and shroud occurs at the lower frequencies, the correlation coefficient increasing sharply at 500 Hz when frequency is decreased.

(e) Correlation coefficients relating trailing edge and free field are similar for flap and shroud.

(f) For the location of maximum correlation on the flap, the highest correlation at 500 and 1000 Hz occurs at microphone 6 (274°), but for 2000, 4000 and 8000 Hz the highest correlation occurs at microphones 3-5 (i.e. 80° to 150°).

(g) Correlation data associated with locations 25 on the flap and 44 on the shroud, where there is only induced flow, did not appear to be significantly different from data for other locations. However the local flow speeds at these locations may be fairly high, especially at location 25

(h) When tunnel flow is introduced, no significant change is observed in far field acoustic pressure levels. However, on the flap and shroud there is a decrease of about 4 dB in spectrum levels below 1000 Hz, measured near the trailing edges. Depending on location and frequency, the correlation coefficient for surface and far field pressures may show an increase or a decrease when tunnel flow is introduced. The general trend is for the correlation coefficient to decrease at low frequencies (500 and 1000 Hz), and increase (or remain unchanged) at higher frequencies, when tunnel flow is introduced. However, if the correlation data are averaged over all surface locations and all octave bands in the range 1000 to 8000 Hz, there is no net change in correlation coefficient associated with the presence of tunnel flow.

7.1 Interaction Noise

The reduction in correlation coefficient at the flap and shroud trailing edges, shown in Figures 15-19, raises the question of the influence of transducer vibration. Measurements of surface pressure spectra showed that these trailing edge locations were the most susceptible to vibration-induced signals. There are, however, three factors which suggest that the reduced correlation may not be associated with vibration effects. The factors are:

(i) The pressure correlations were measured when the vibration-induced peaks in the surface pressure spectra had been reduced to a minimum.

(ii) Spectra at location 14 were also strongly influenced by vibration effects, yet the correlation coefficients are higher than at the trailing edge.

(iii) Data of Scharton et al [6] for flow over a single plate show a similar reduction in surface-far field correlation

coefficient at the trailing edge, with the higher frequencies having maximum correlation nearer to the trailing edge.

Scharton et al compare the location of maximum correlation coefficient with estimates of source size. They show reasonable agreement at 8 and 16 kHz, but not at 2 and 4 kHz. A similar procedure can be followed here.

From Figure 20(b) the maximum correlation coefficient at frequencies 1 kHz to 4 kHz is 0.1. Using equation (8), the number of independent acoustic sources is

$$N = 100 \quad .$$

Assuming these sources to be distributed in a single spanwise array, the source size is 0.76 cm (0.3"), since the model span is 76 cm (30"). This dimension is similar to the spanwise length scale Λ_3 at the flap leading edge (Table II) but only 25% of the value of Λ_3 at the flap trailing edge. The above source size is also similar to the distance between the region of maximum correlation and the flap trailing edge, 0.63 to 1.27 cm (0.25" to 0.5"). Thus the result is similar to that of Scharton et al.

Proceeding further, since the pressure field on the flap is convected downstream at a speed of 204 m/s (670 ft/sec), the wavelength at 2000 Hz is 10.2 cm (4.0"). This wavelength is about eight times larger than the distance between the location of maximum correlation and the flap trailing edge.

Far field sound spectra for the augmentor wing can be compared with similar spectra measured during early tests on the nozzle alone. Such a comparison is shown in Figure 28, where the angle θ refers to the thrust axis in each case. The presence of the augmentor seems to cause a redistribution of the sound power at frequencies above about 5000 Hz. This may be due to shielding by the flap and shroud. At angles of about 90° there is a marked increase in low frequency sound, which may be associated with trailing edge noise.

Typical frequencies associated with broadband noise from the flap trailing edge can be estimated from Hayden [8]. The Strouhal number $f\delta/U$ for the spectral peak has a value in the range 0.04 to 0.06. In the absence of detailed flow information, upper bounds are assumed for both δ and U, with δ being taken as half the distance between flap and shroud trailing edges and $U = U_j$, the jet velocity. The resulting peak frequency lies in the range 400-650 Hz, i.e. it is below 1000 Hz.

7.2 Jet Noise

Before drawing conclusions regarding the noise sources of the augmentor wing, it is necessary to consider the role played by the jet. Scharton et al [6] have observed that the pressure spectrum at the jet boundary of a model jet changed little when a flat plate was introduced. Source locations in the jet (Table IV) can be estimated from results of MacGregor and Simcox [9], taking the nozzle height as the scale dimension.

The contents of Table IV indicate that, for a free jet, sound at 500 and 1000 Hz would be generated at axial distances which are downstream of the flap trailing edge. Acoustic energy at frequencies 2000-8000 Hz would be generated mainly within the augmentor, between flap mid-chord and trailing edge.

Table IV

Estimated Locations of Acoustic Sources in Augmentor Jet

Frequency (Hz)	500	1000	2000	4000	8000	16000
Source Location x_s (cm)	29.2	23.6	19.0	15.5	12.4	9.9
(inch)	11.5	9.3	7.5	6.1	4.9	3.9
x_s/x_f	1.44	1.16	0.94	0.76	0.61	0.49

(x_f = flap chord)

A similar result is obtained when noise source locations are estimated for the 172 lobe augmentor system used by Campbell et al [1]. Furthermore reference [1] presents spectra showing the far field noise reduction achieved when acoustic absorbing material is placed on the surfaces of the flap and shroud. The results are summarized in Figure 29 where it is seen that no noise reduction is achieved at frequencies below 2000 Hz. This finding is consistent with above estimates of noise source locations in the free jet.

Correlation of surface pressures on the flap indicated the presence of pressure components at 2000 and 4000 Hz which were convected in the upstream direction. These components can be attributed to acoustic rather than aerodynamic pressures. Values of the correlation coefficient associated with these acoustic pressures are typically 0.05. If it is assumed that (1) the aerodynamic and acoustic pressures are uncorrelated and (2) the sound waves do not decay within the augmentor, then the data can be taken as indicating that

$$\overline{p}^2(\text{acoustic}) \approx 0.05\ \overline{p}^2(\text{aerodynamic})$$

i.e. there is a 13 dB difference in mean square levels. Under idealized conditions this could result in a surface-far field correlation coefficient of 0.05, a value which is typical of the measured coefficients.

8. CONCLUSIONS

Noise generation mechanisms for an augmentor wing can be considered in two frequency regions.

(a) High frequencies: jet noise components are generated within the augmentor and the noise levels are typically 15 dB below the fluctuating aerodynamic pressures on the flap and shroud. However the jet noise is the dominant source of far field sound levels for an untreated augmentor. When acoustic treatment is added, interaction noise from the trailing edges of the flap and shroud may become important.

(b) Low frequencies: jet noise levels are generated outside the augmentor, and flow-surface interaction noise is generated at the trailing edges of the flap and shroud.

The role of freestream flow velocity is not well defined, but on the average there is little change in far field sound levels and in the correlation between surface and far field locations.

It is recommended that the following items be considered in designs for reducing far field noise levels of an augmentor wing:

(a) For low frequencies: increase the length of the augmentor flap and shroud and add acoustic treatment which is effective at low frequencies; design porous, or other, trailing edges to reduce interaction noise.

(b) For high frequencies: optimize treatment for maximum attenuation; obtain maximum possible benefit from trailing edge designs, at high frequencies. At very high frequencies minimize the acoustic leakage at the leading edges of the flap shroud.

REFERENCES

1. Campbell, J. M., Lawrence, R. L., O'Keefe, J. V., "Design integration and noise studies for jet STOL aircraft. Final Report, Volume IV, Static Test Program." NASA CR-114285, May 1972.

2. Siddon, T. E., "Surface dipole strength by cross-correlation method." *J. Acoust. Soc. Am.* **53**, 2, 620-633, February 1973.

3. White, P. H., "Cross correlation in structural waves: Dispersion and nondispersion waves." *J. Acoust. Soc. Am.* **45**, 5, 1118-1128, May 1969.

4. Bull, M. K., "Wall-pressure fluctuations associated with subsonic turbulent boundary layer flow." *J. Fluid Mech.* **28**, Part 4, 719-754, June 1967.

5. Maestrello, L., Gedge, M. R., Reddaway A. R. F., "The response of a simple panel to the pseudo-sound field of a jet." 189-208, *Aerodynamic Noise*, Editor H. S. Ribner, University of Toronto Press, 1969.

6. Scharton, T. D., Pinkel, B., Wilby, J. F., "A study of trailing edge blowing as a means of reducing noise generated by the interaction of flow with a surface." NASA CR-132270, Contract No. NAS1-9559 (BBN Report 2593), September 1973.

7. Stone, J. R., "Interim prediction method for jet noise." NASA TM X-71618.

8. Hayden, R.E., "Noise from interaction of flow with rigid surfaces: A review of current status of prediction techniques." NASA CR-2126 (Contract NAS1-9559-14) BBN Report 2276, April 1973.

9. MacGregor, G.R., Simcox, C.D., "The location of acoustic sources in jet flows by means of the "wall isolation" technique." AIAA Paper 73-1041, Seattle , Washington, October 1973.

10. Fuchs, H.V., "Space correlations of the fluctuating pressure in subsonic turbulent jets" J. Sound Vib. 23, 1, 77-99, July 1972.

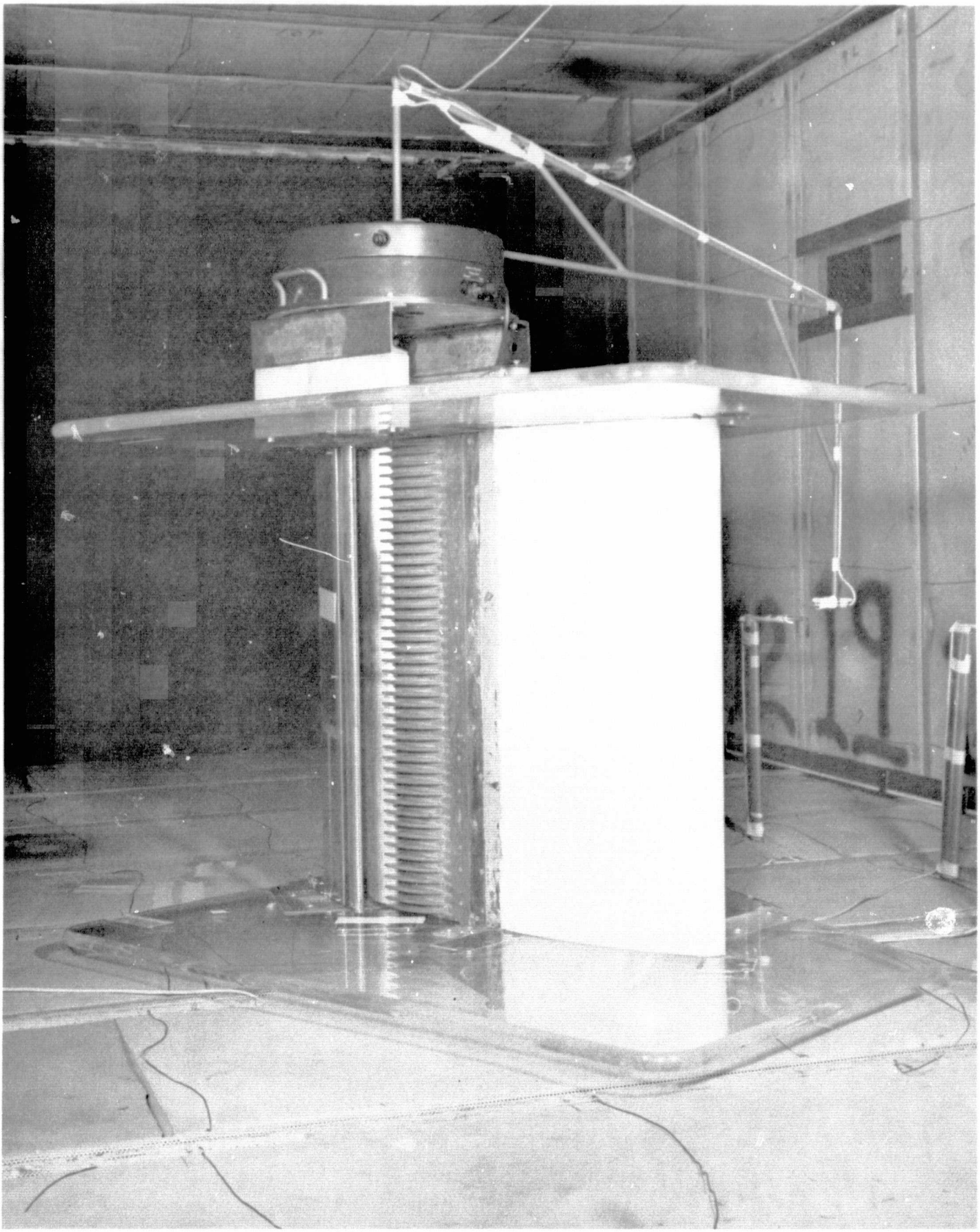

FIGURE 1. MODEL SCALE AUGMENTOR WING IN TUNNEL TEST SECTION

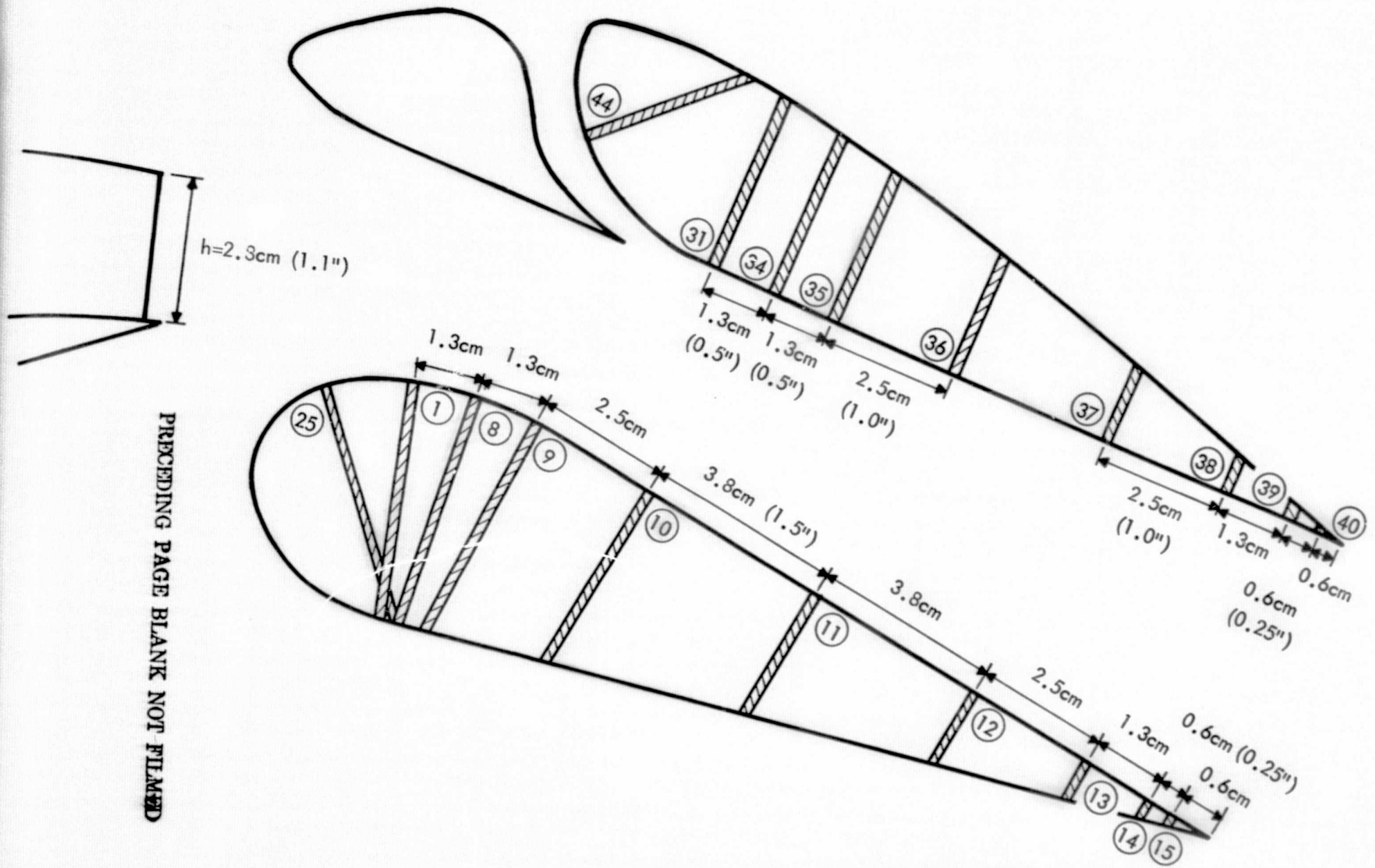

FIGURE 2a. LOCATION OF SURFACE PRESSURE TRANSDUCERS ON FLAP AND SHROUD (CROSS-SECTION)

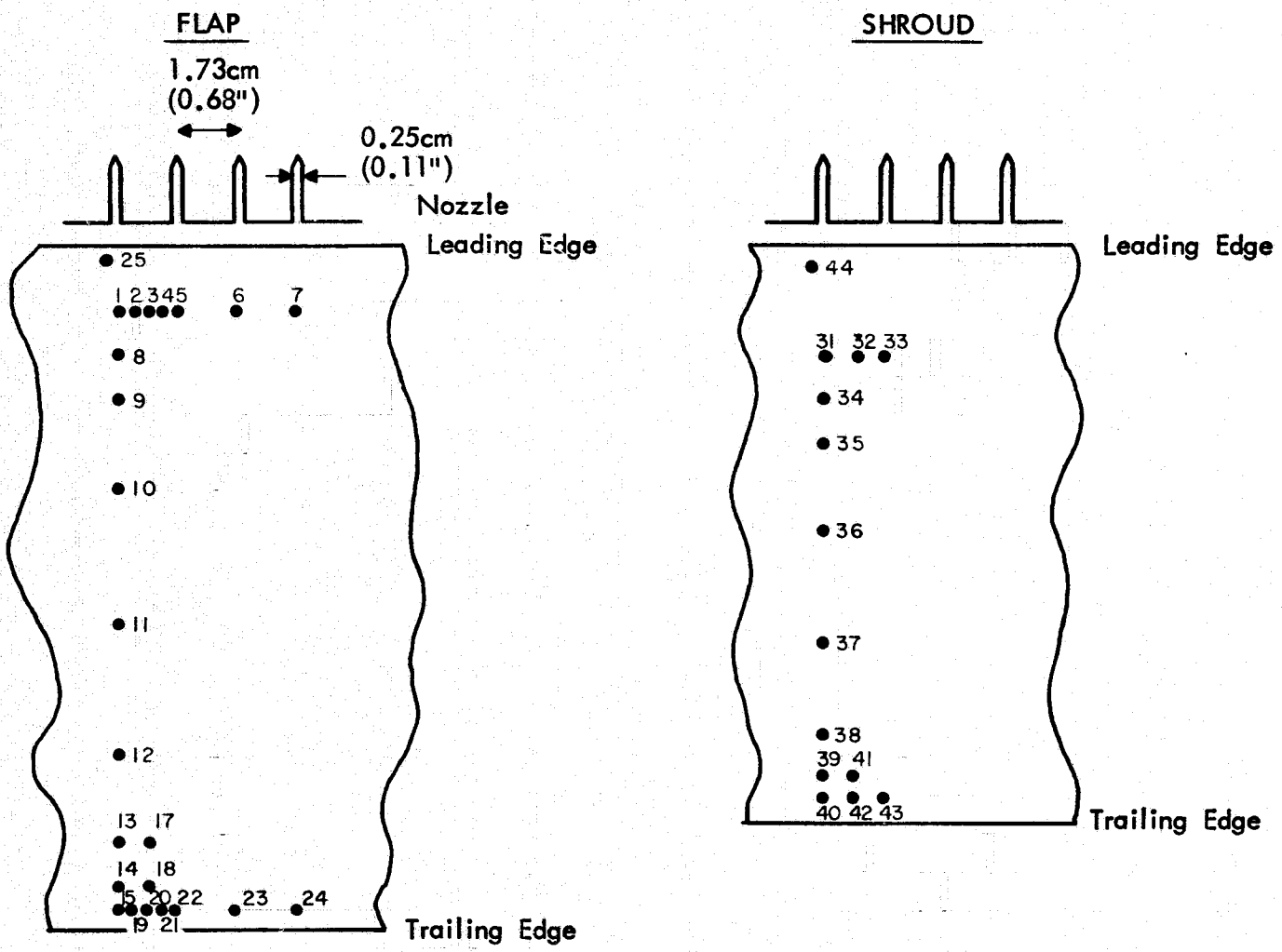

FIGURE 2b. TRANSDUCER LOCATIONS ON FLAP AND SHROUD (PLAN VIEW)

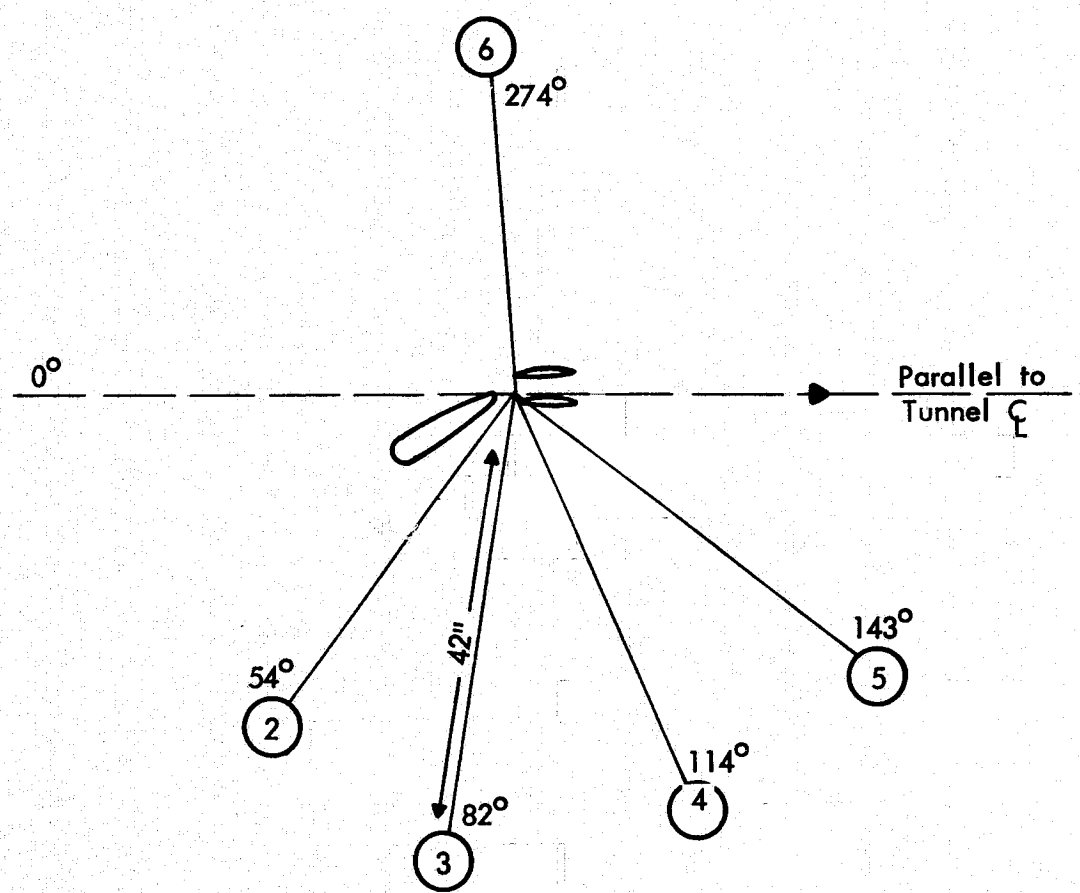

FIGURE 3. FAR-FIELD MICROPHONE LOCATIONS WITH AUGMENTOR INSTALLED

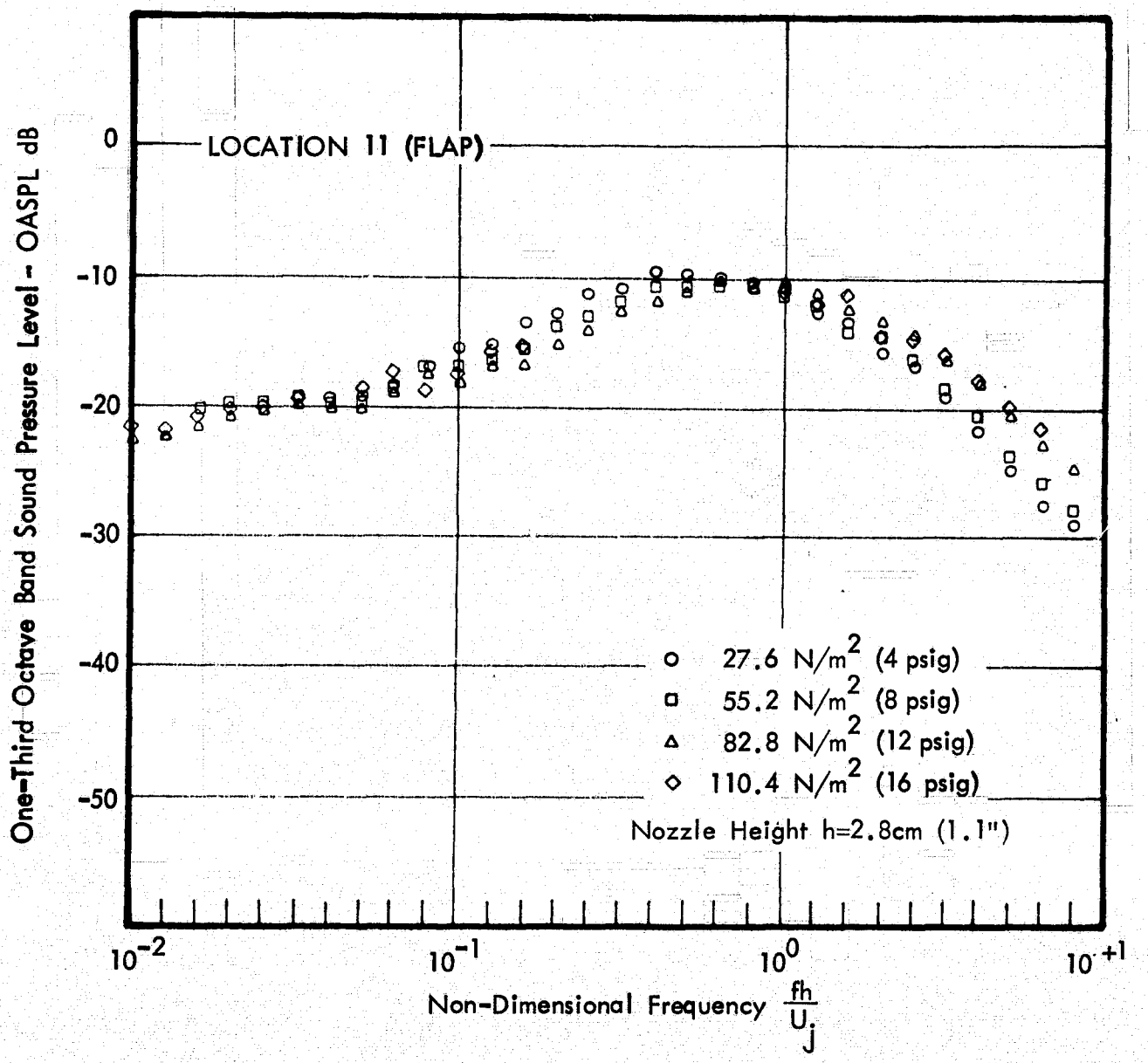

FIGURE 4. NON-DIMENSIONAL SURFACE PRESSURE SPECTRA AT LOCATION 11 ON FLAP

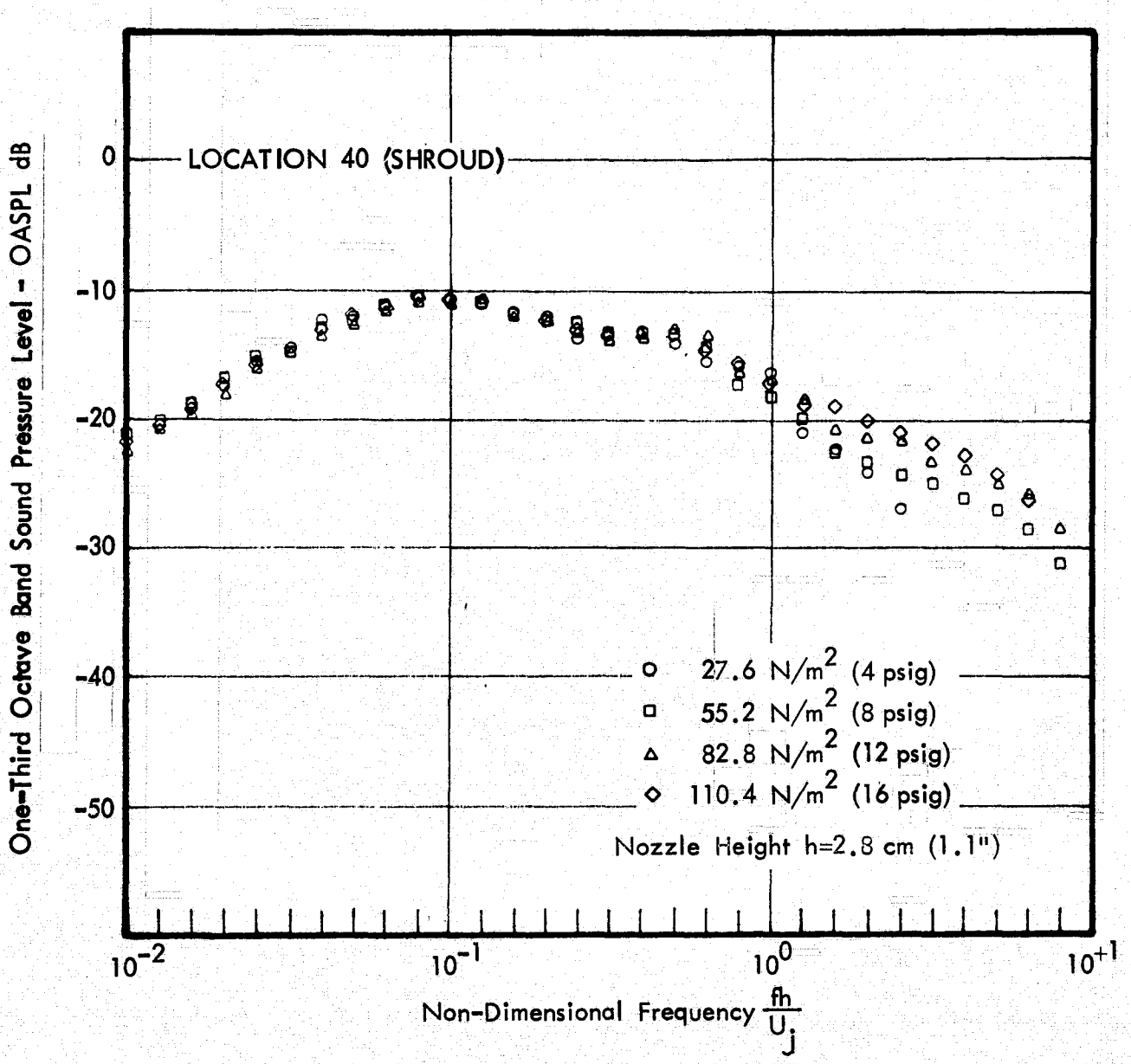

FIGURE 5. NON-DIMENSIONAL SURFACE PRESSURE SPECTRA AT LOCATION 40 ON SHROUD

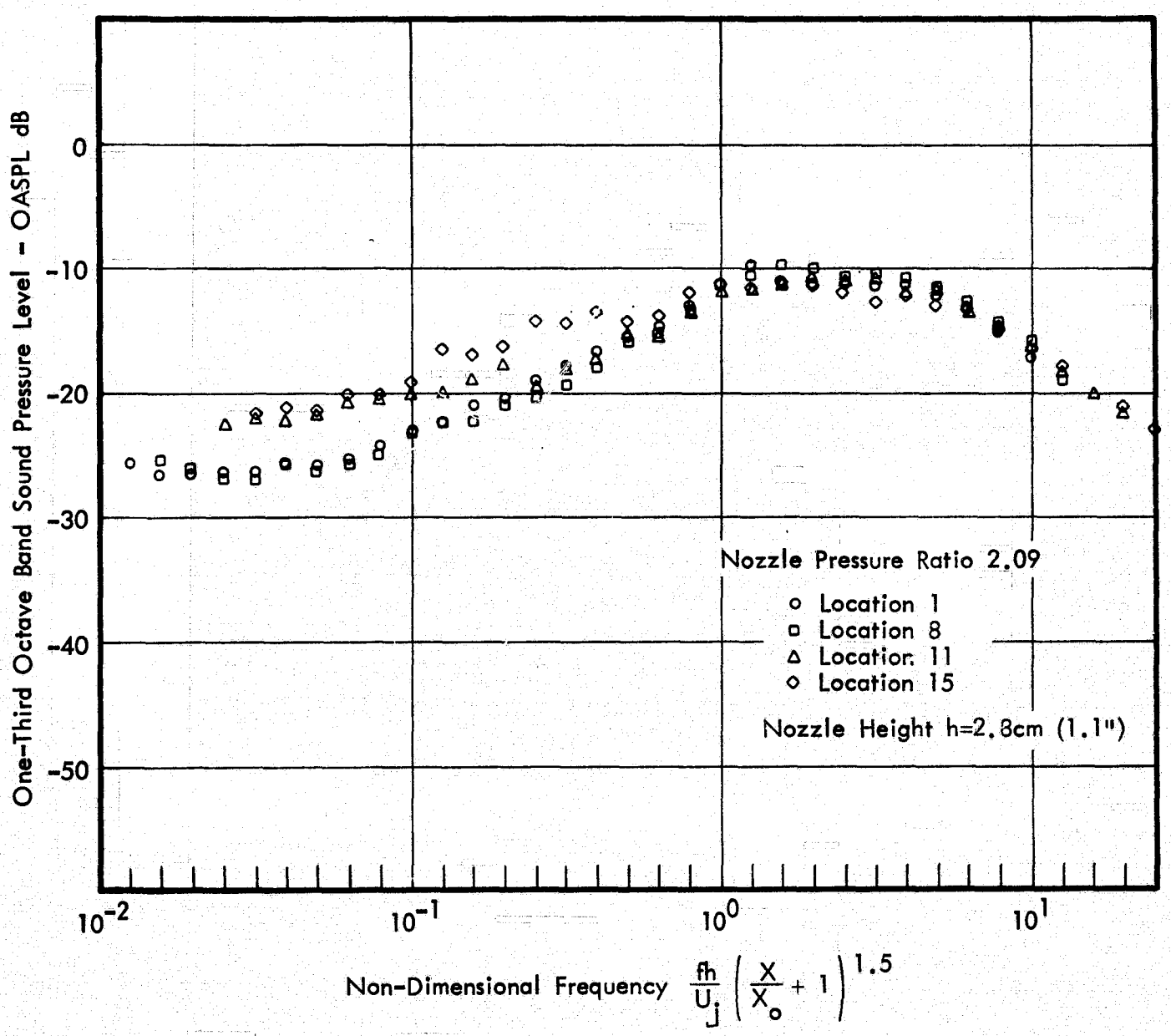

FIGURE 6. NON-DIMENSIONAL PRESSURE SPECTRA AT DIFFERENT CHORDWISE LOCATIONS ON SURFACE OF FLAP

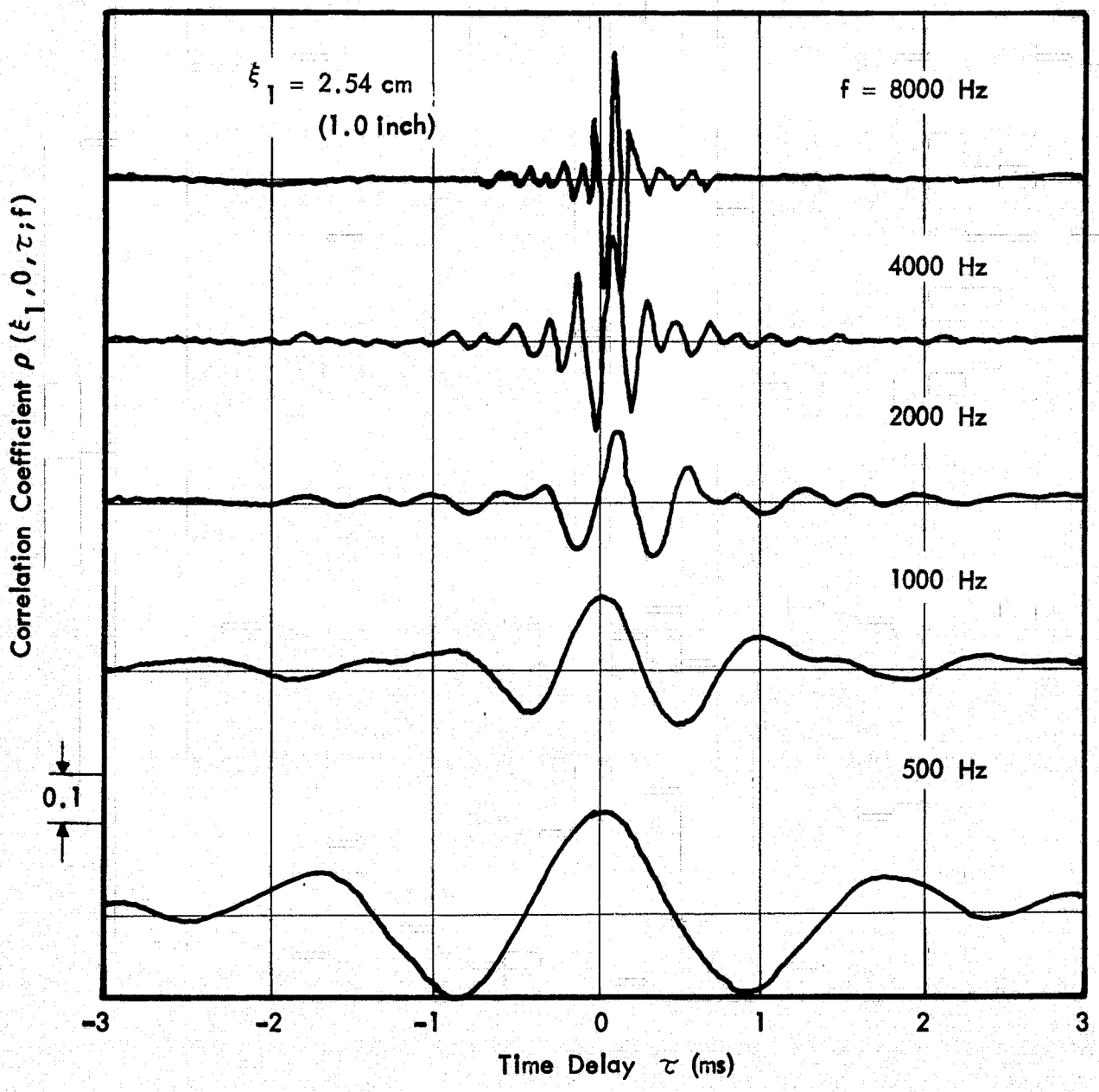

FIGURE 7. TYPICAL OCTAVE BAND CORRELATION COEFFICIENTS FOR SURFACE PRESSURES ON FLAP

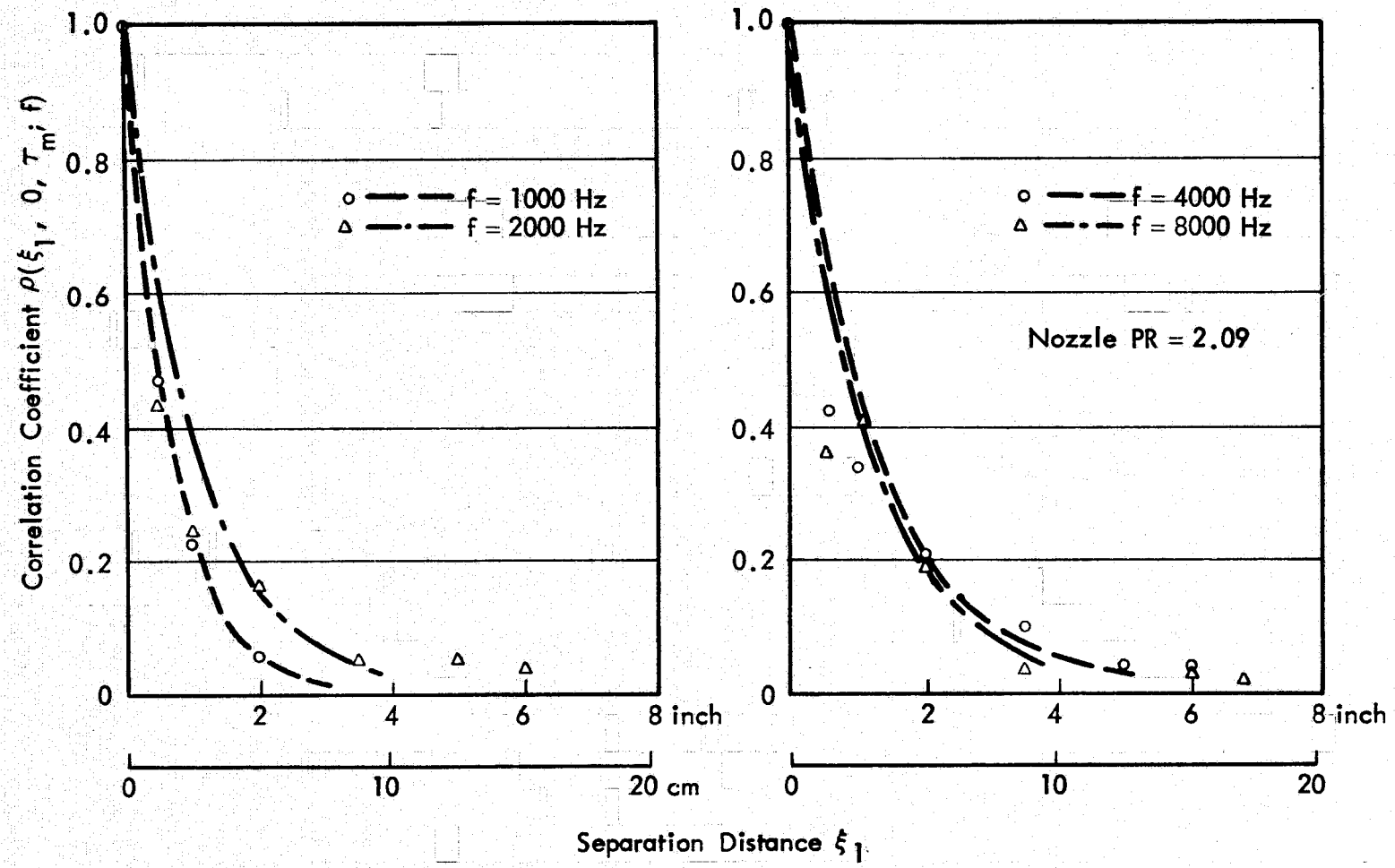

FIGURE 8. MOVING FRAME CHORDWISE PRESSURE CORRELATIONS ON FLAP

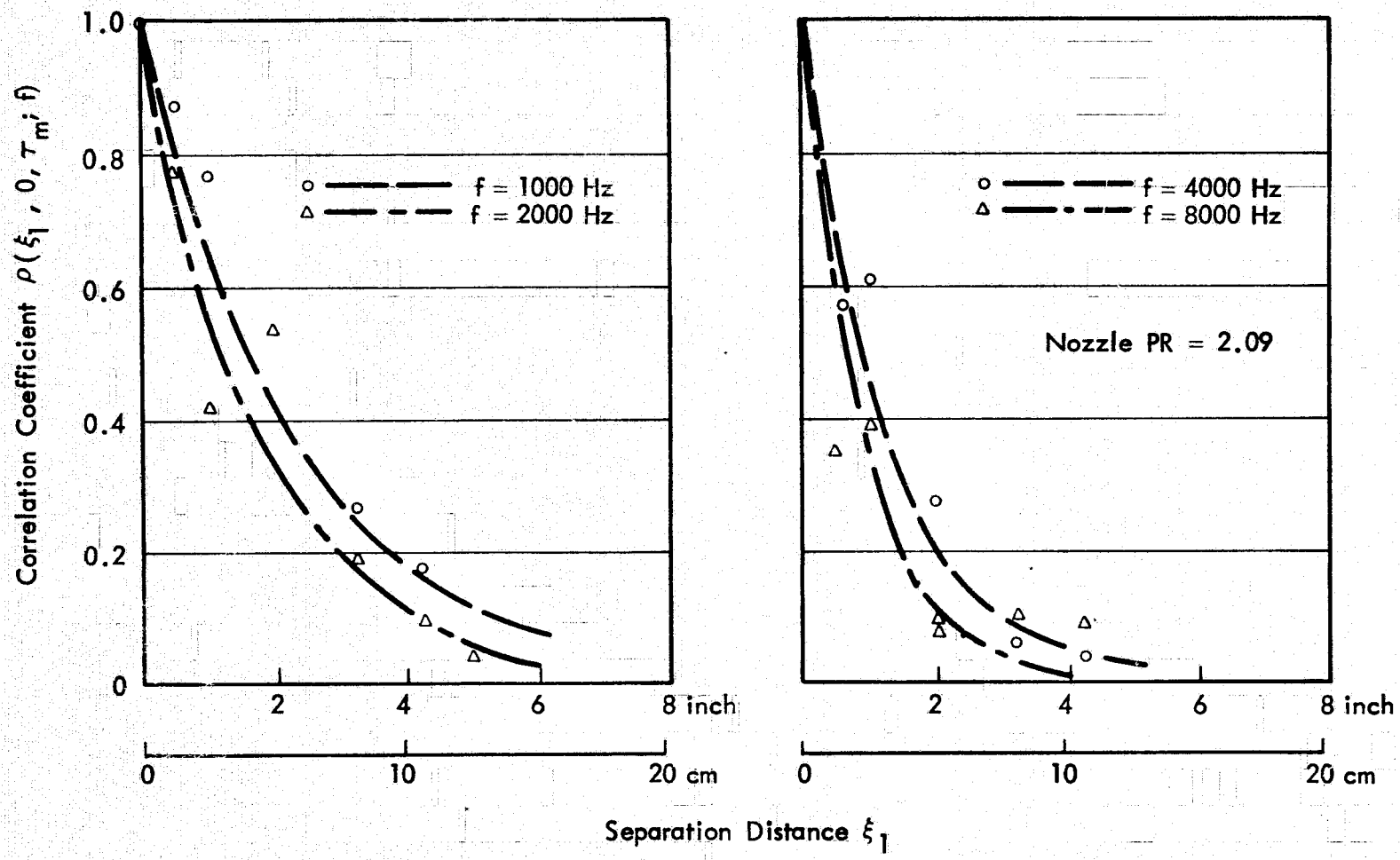

FIGURE 9. MOVING FRAME CHORDWISE PRESSURE CORRELATIONS ON SHROUD

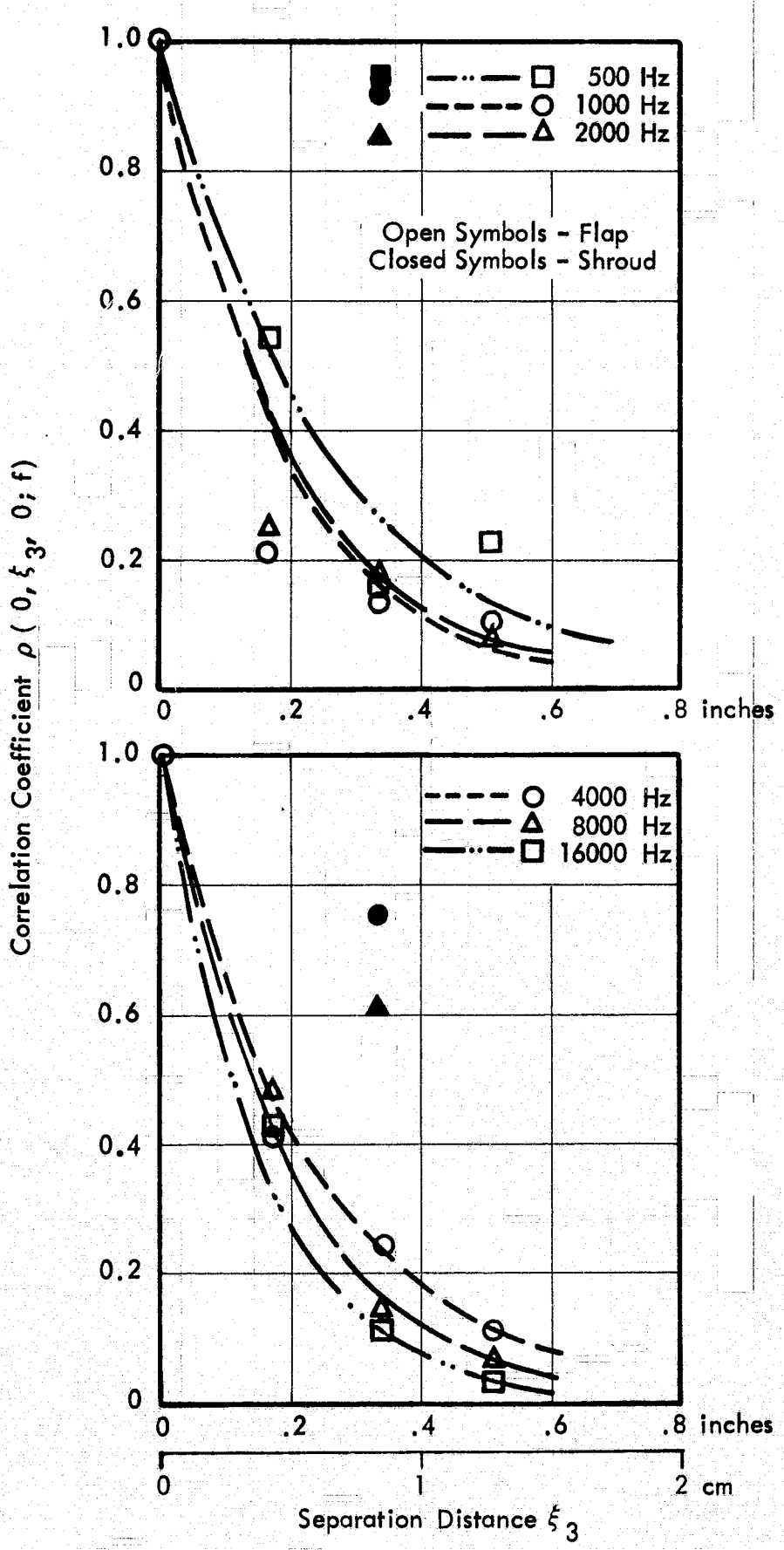

FIGURE 10. SPANWISE SPACE CORRELATION COEFFICIENT FOR PRESSURES ON FLAP AND SHROUD LEADING EDGES

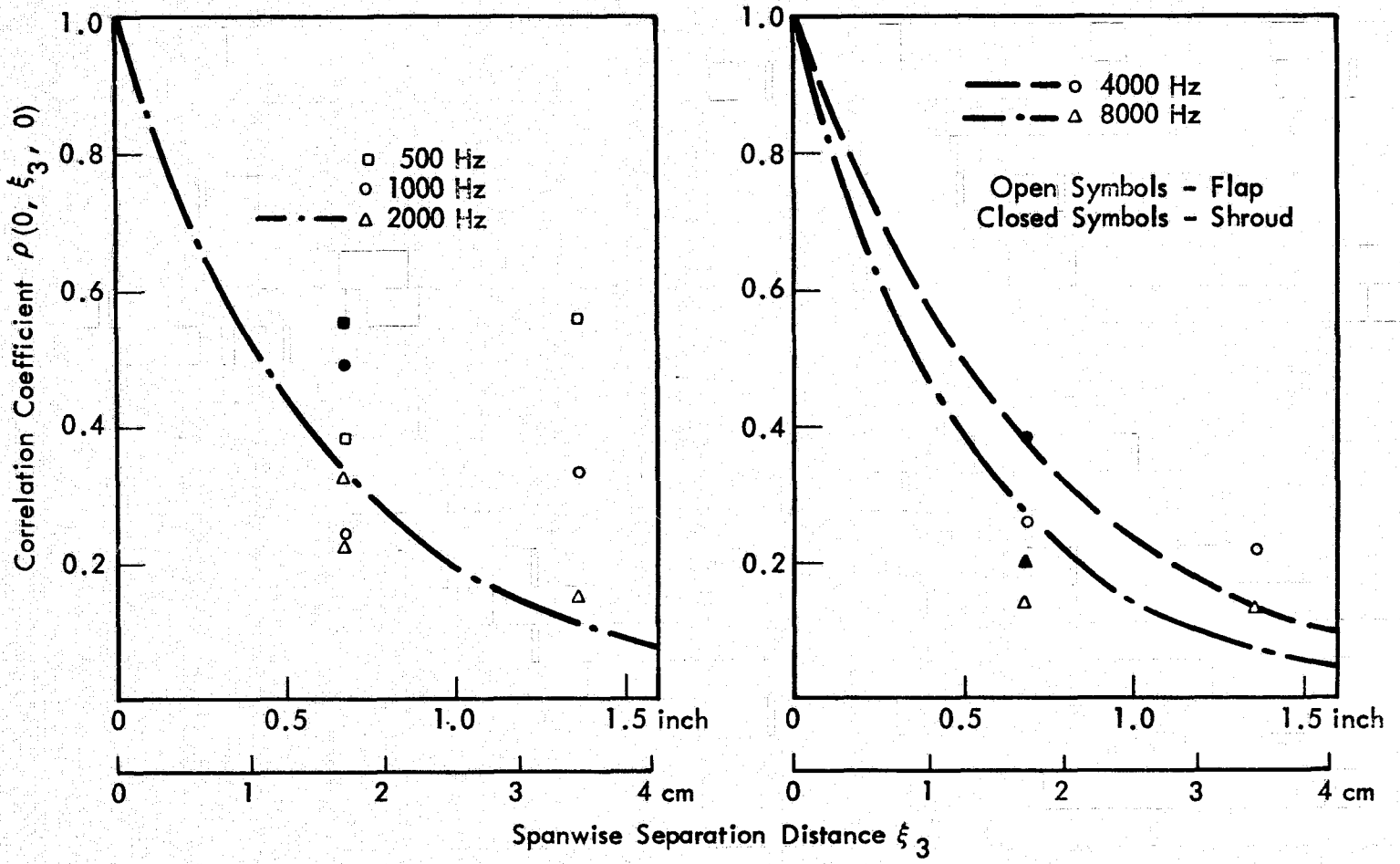

FIGURE 11. SPANWISE SPACE CORRELATION COEFFICIENT FOR PRESSURES ON FLAP AND SHROUD TRAILING EDGES

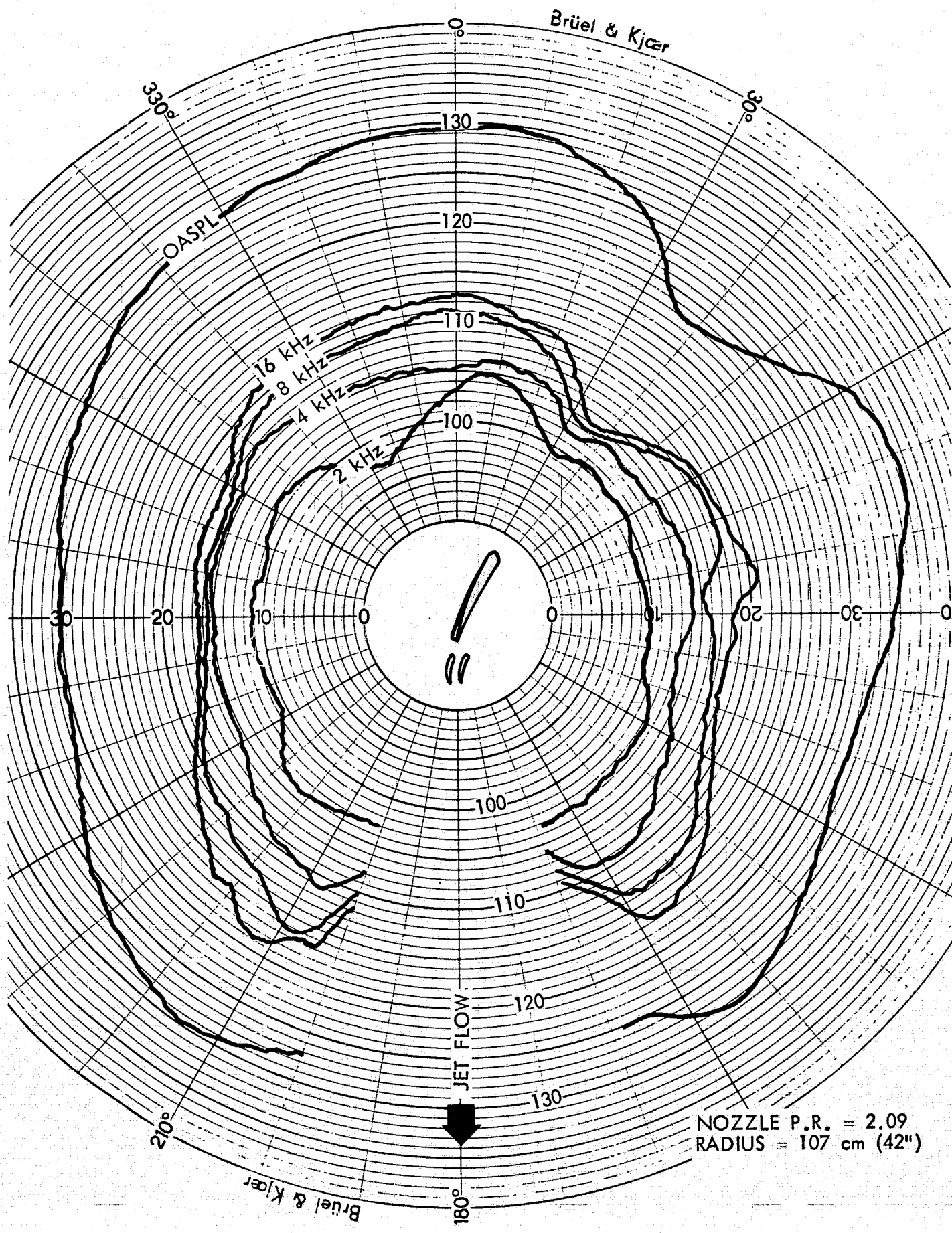

FIGURE 12. POLAR PLOT OF ACOUSTIC FAR FIELD OF AUGMENTOR WING

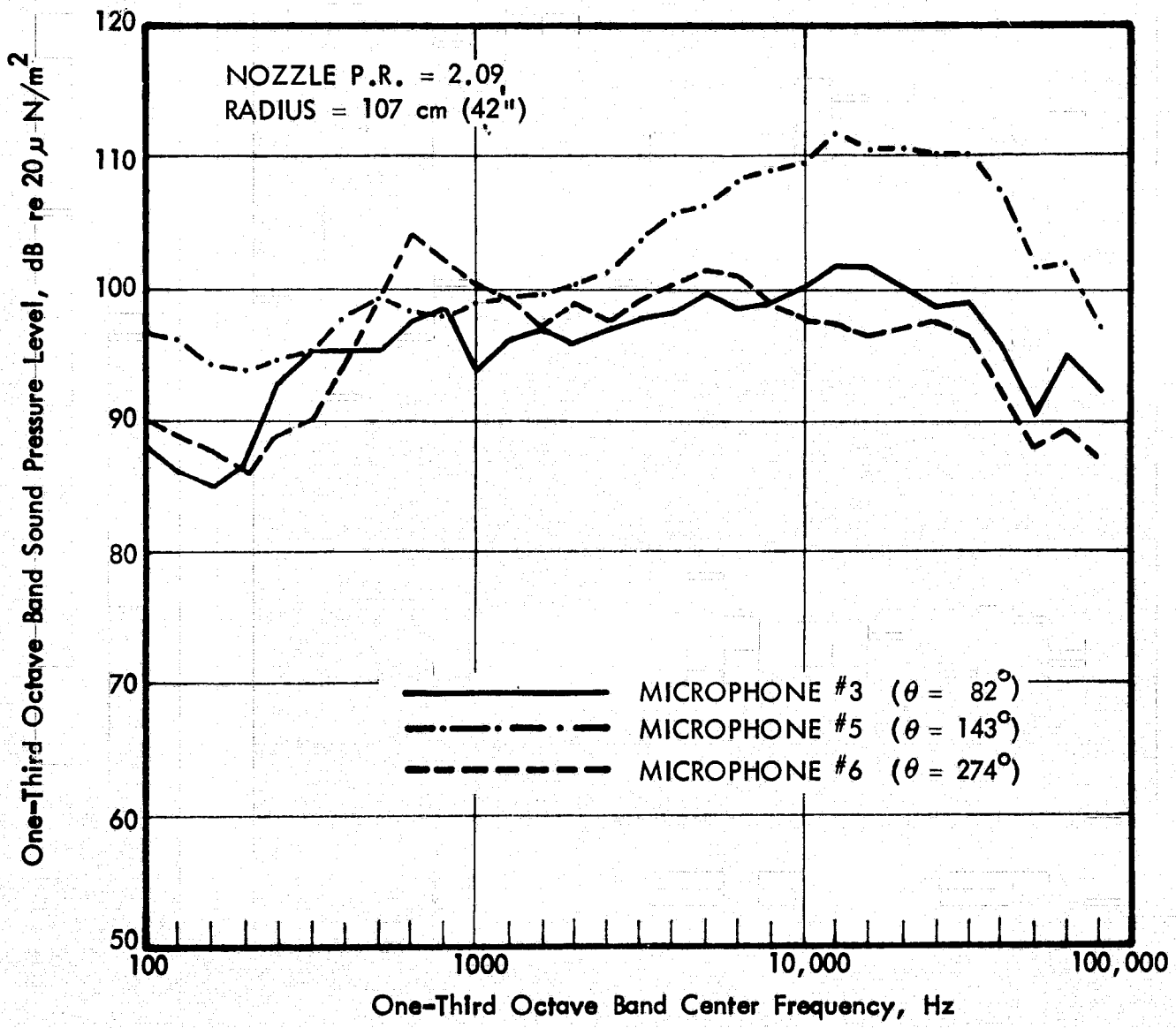

FIGURE 13. ACOUSTIC FAR FIELD SPECTRA FOR AUGMENTOR WING (ZERO TUNNEL FLOW)

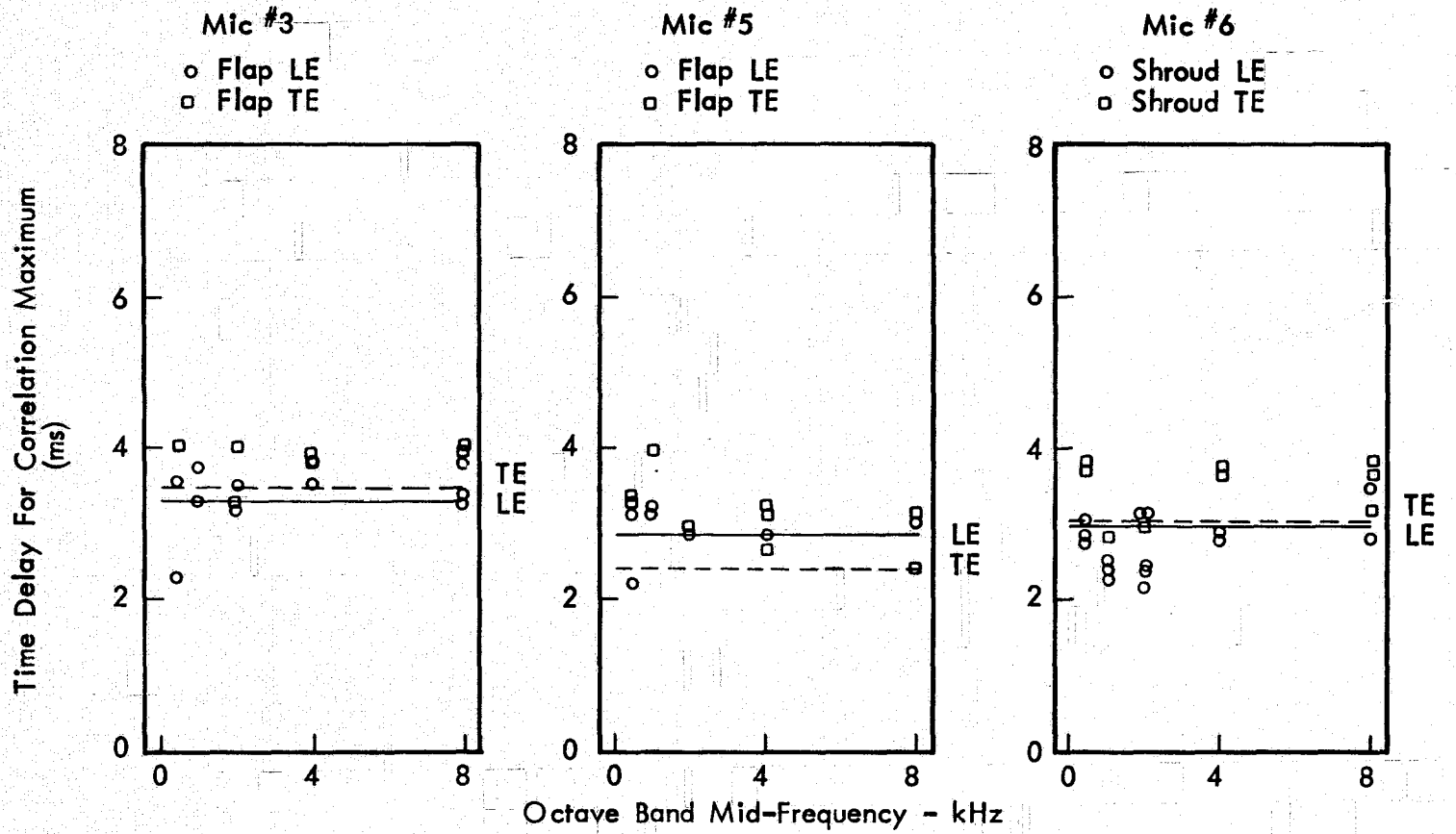

FIGURE 14. TIME DELAY FOR MAXIMA IN SURFACE TO FAR-FIELD PRESSURE CORRELATIONS.

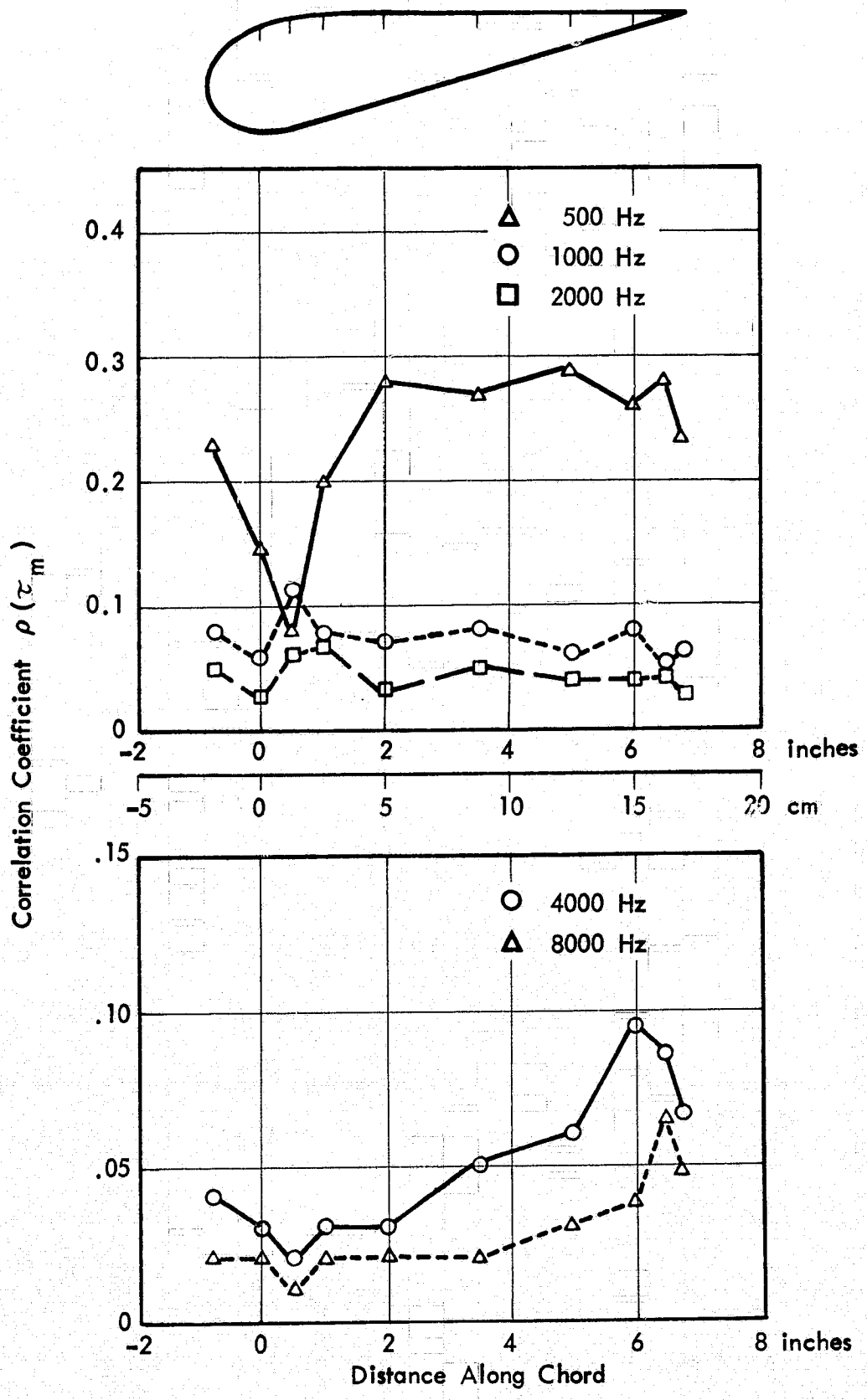

FIGURE 15. FLAP SURFACE - FAR FIELD PRESSURE CORRELATION COEFFICIENT (MICROPHONE 3, θ = 82°)

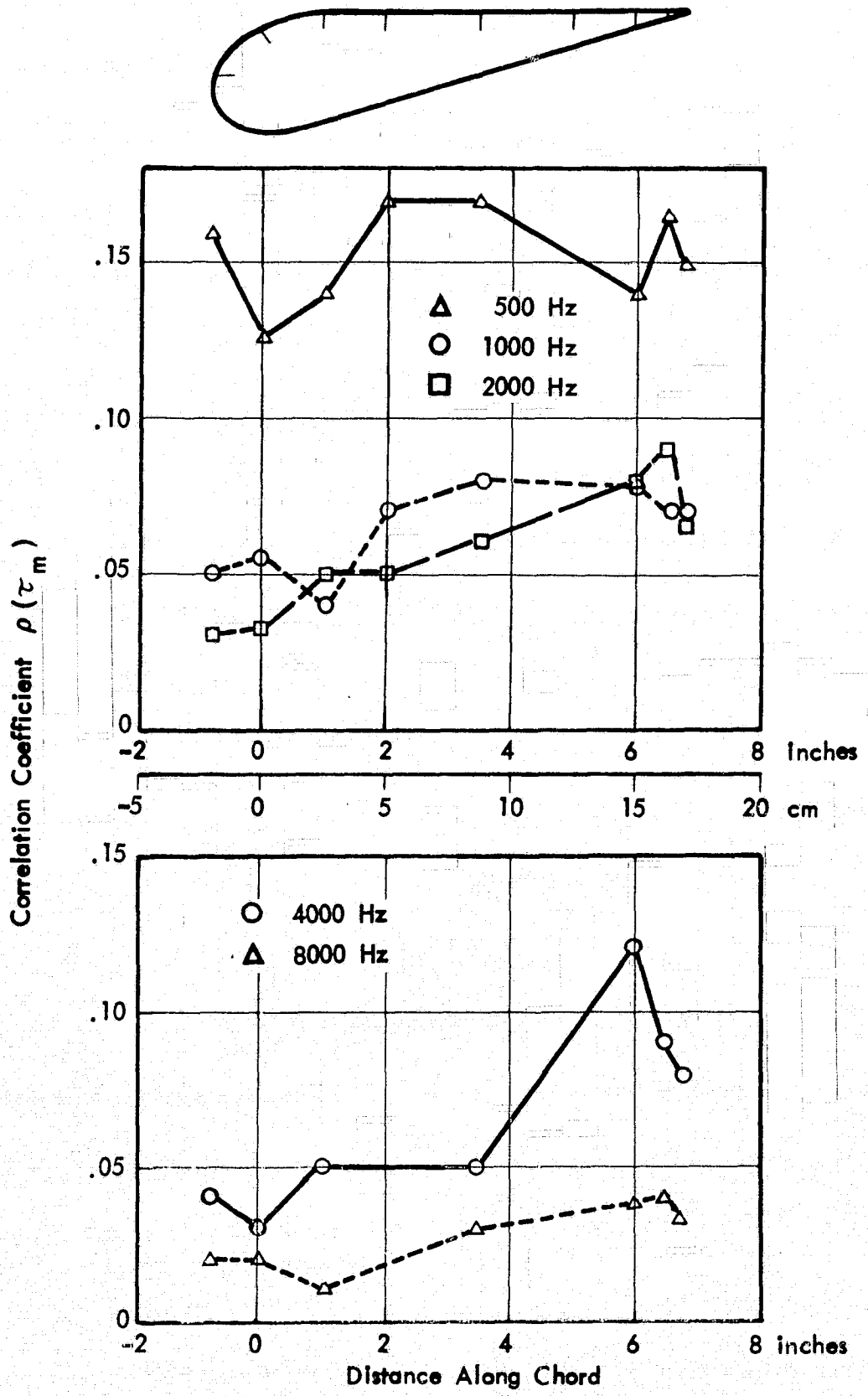

FIGURE 16. FLAP SURFACE - FAR FIELD PRESSURE CORRELATION COEFFICIENT (MICROPHONE 5, θ = 143°)

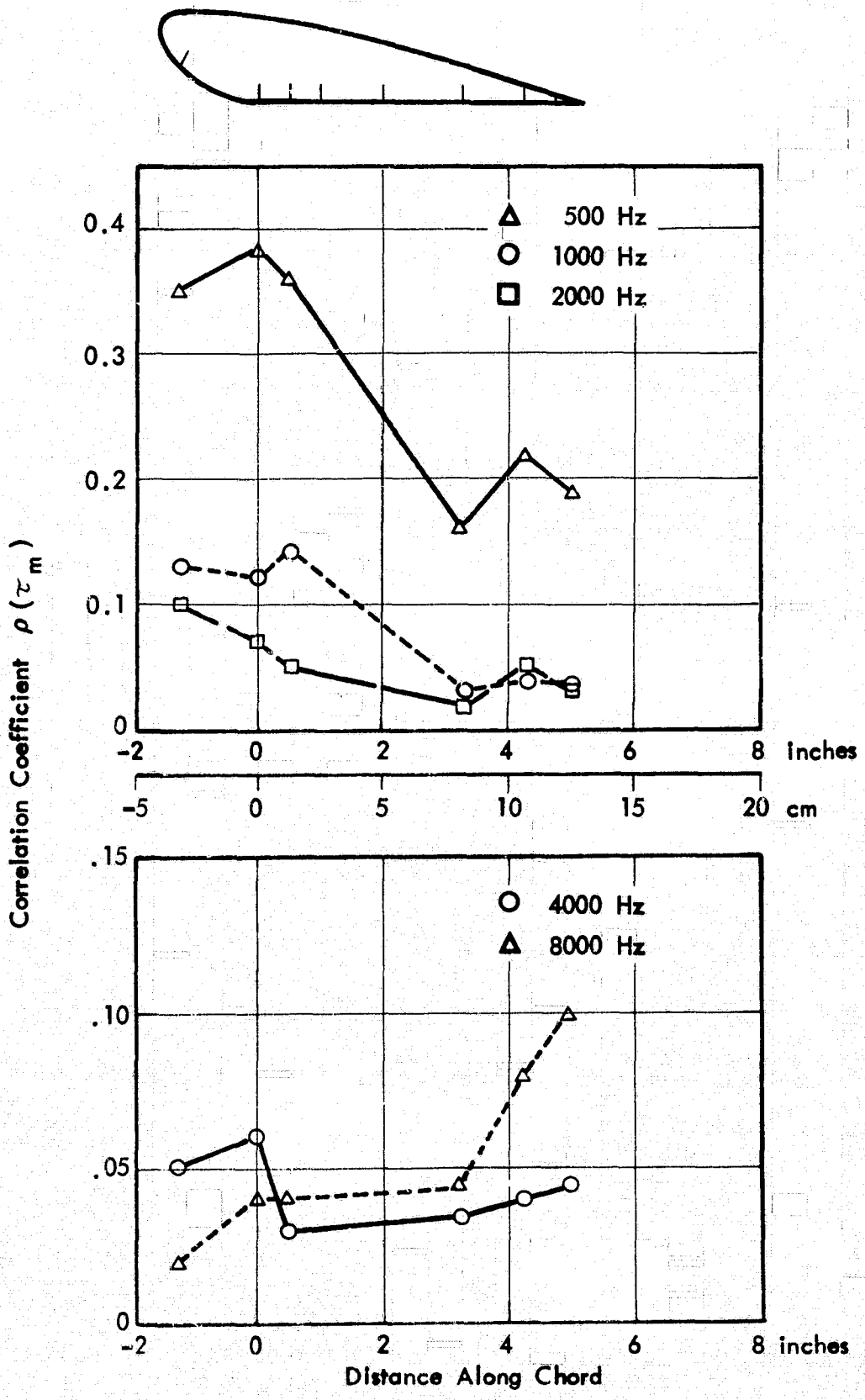

FIGURE 17. SHROUD SURFACE – FAR FIELD PRESSURE CORRELATION COEFFICIENT (MICROPHONE 3, θ 82°)

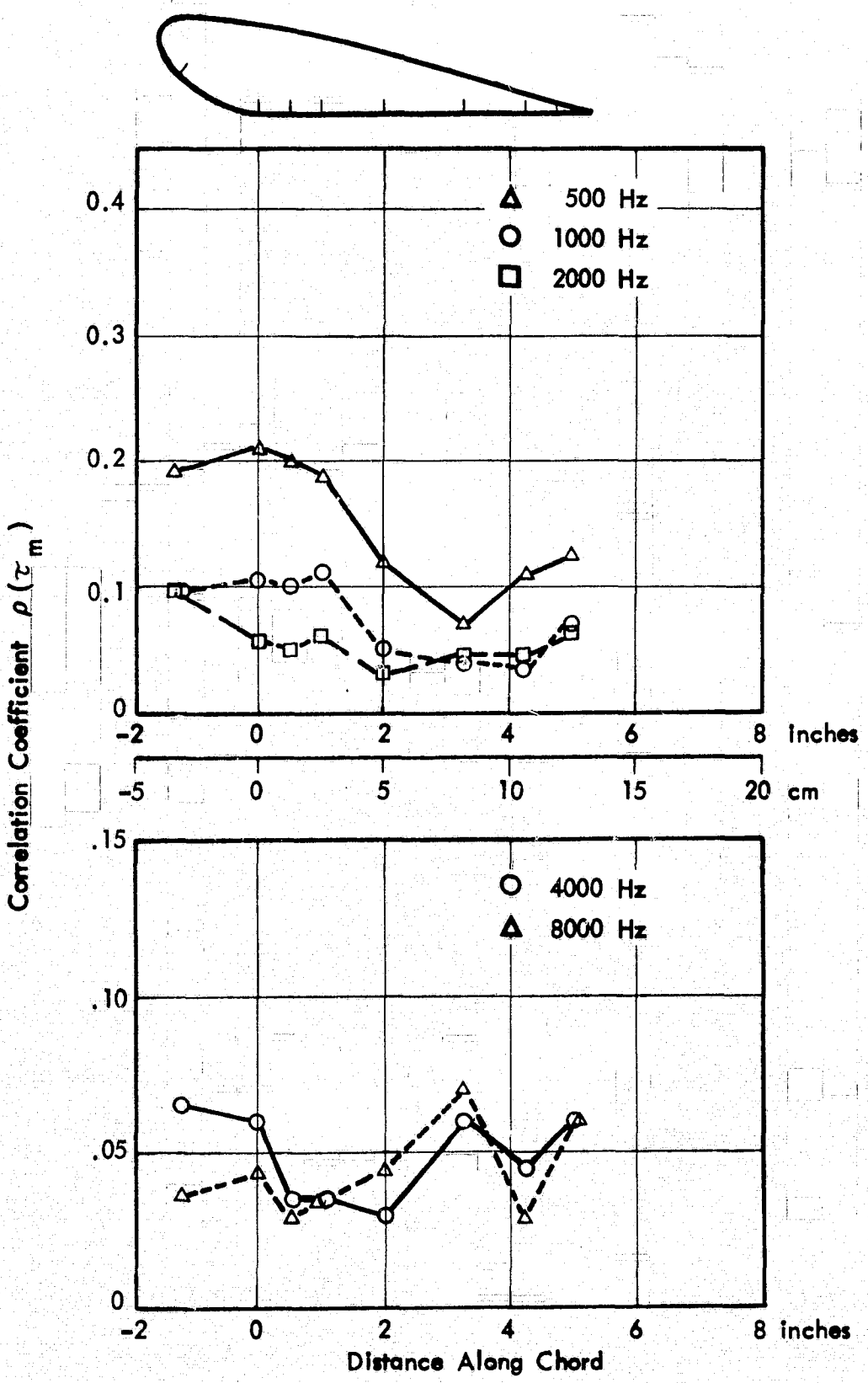

FIGURE 18. SHROUD SURFACE - FAR FIELD PRESSURE CORRELATION COEFFICIENT (MICROPHONE 5, $\theta = 143°$)

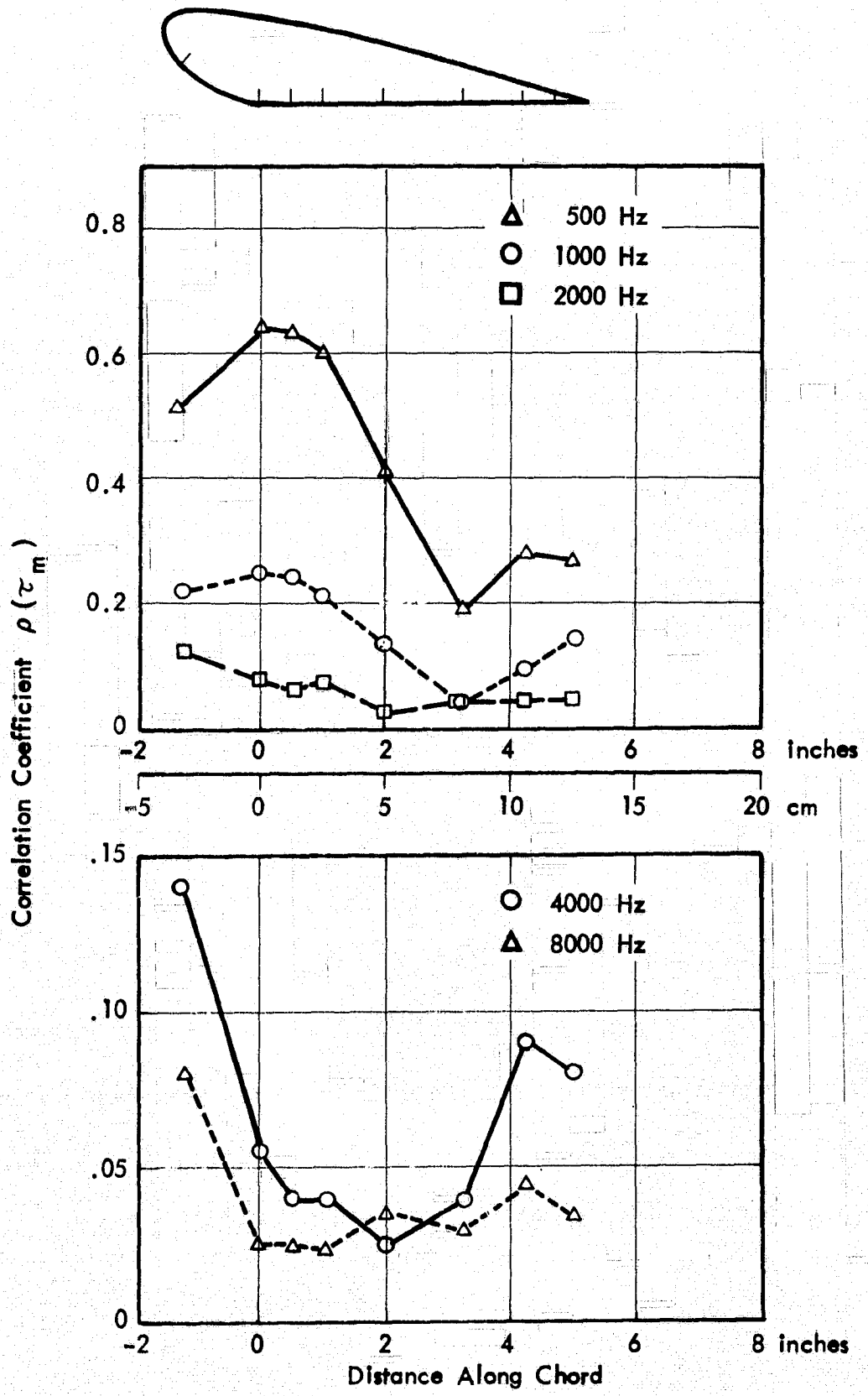

FIGURE 19. SHROUD SURFACE - FAR FIELD PRESSURE CORRELATION COEFFICIENT (MICROPHONE 6, θ = 274°)

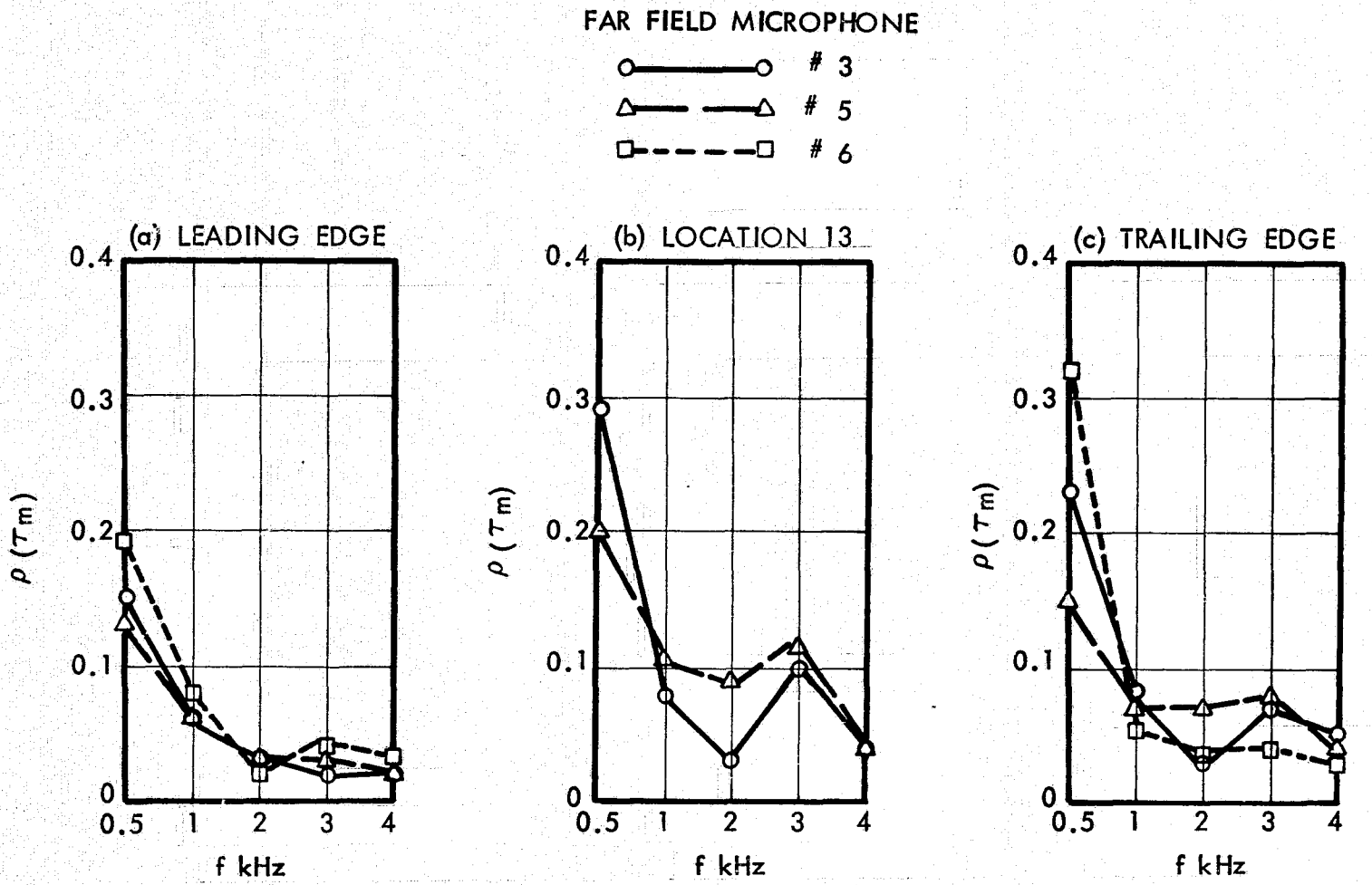

FIGURE 20. FLAP SURFACE - FAR FIELD PRESSURE CORRELATION COEFFICIENT AS FUNCTION OF FREQUENCY

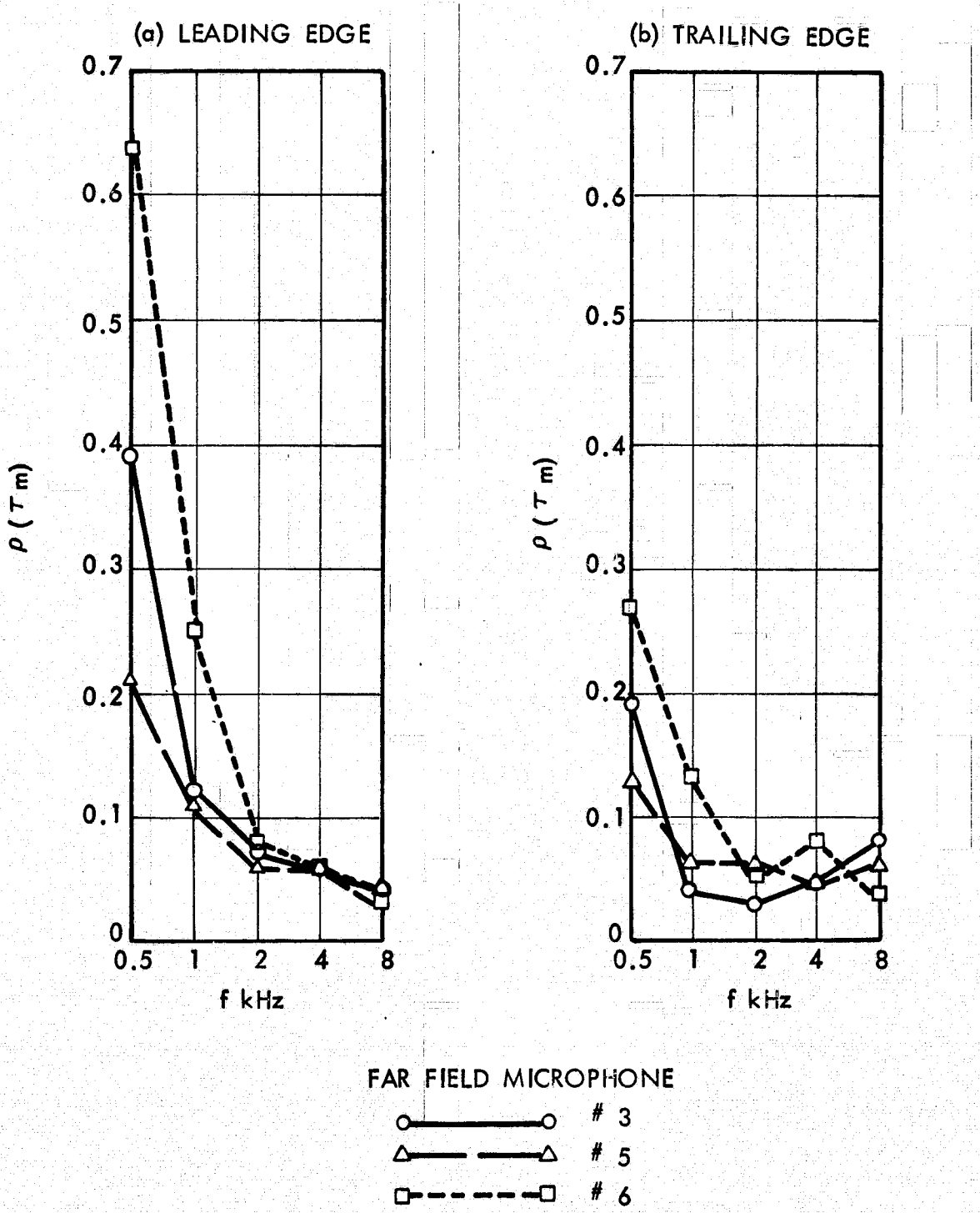

FIGURE 21. SHROUD SURFACE - FAR FIELD PRESSURE CORRELATION COEFFICIENT AS FUNCTION OF FREQUENCY

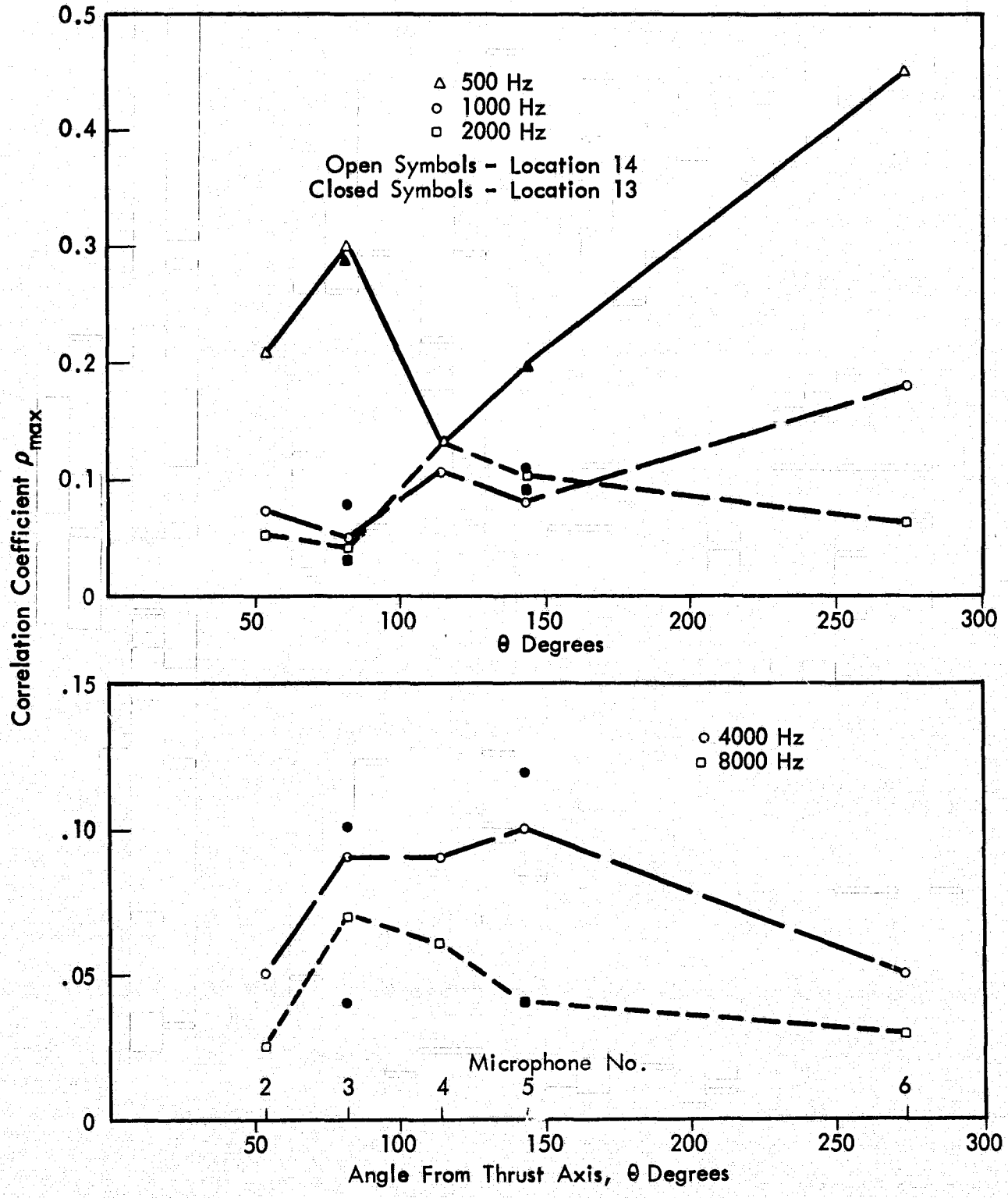

FIGURE 22. ANGULAR VARIATION OF SURFACE - FAR FIELD PRESSURE CORRELATION COEFFICIENT FOR FLAP

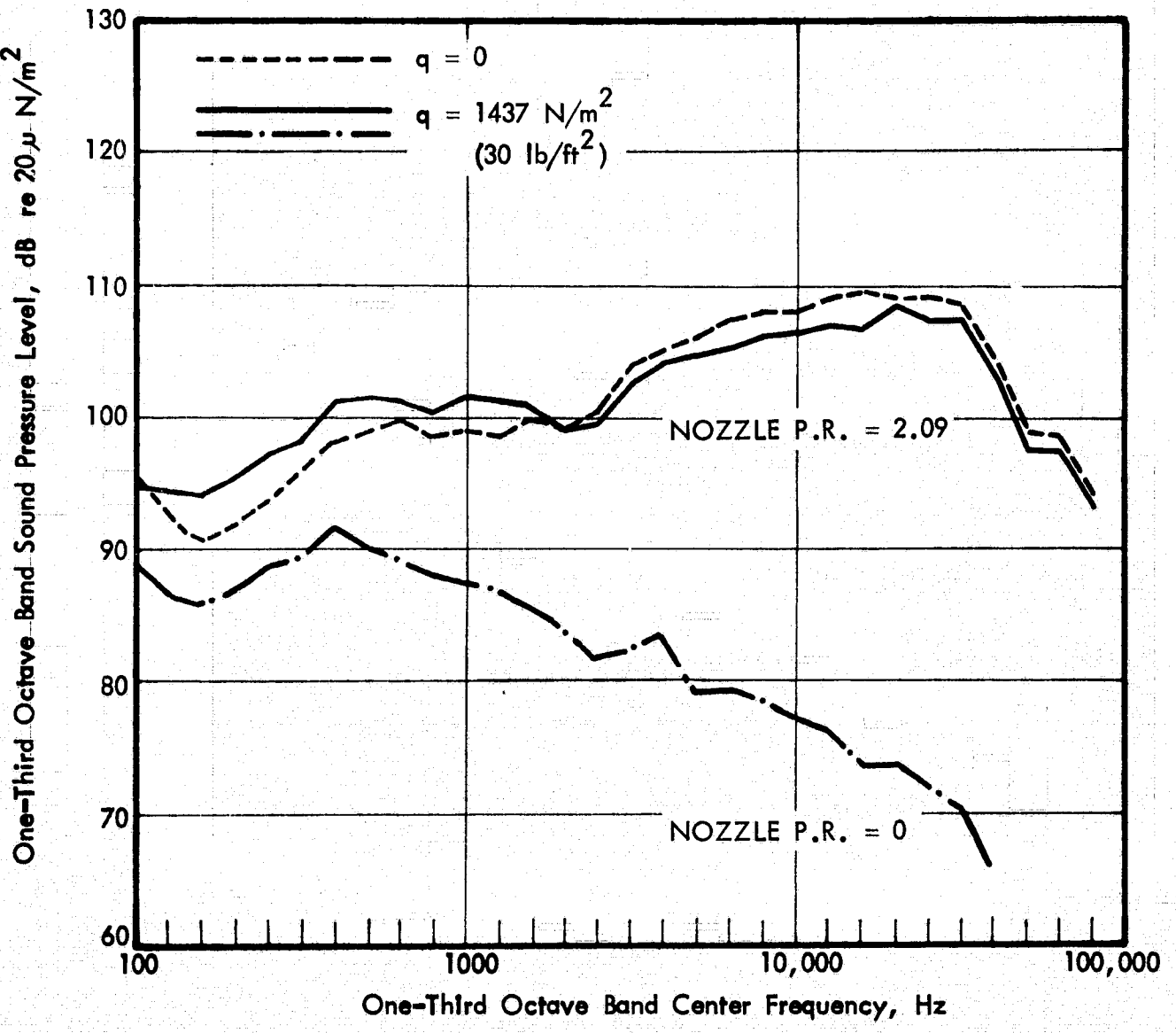

FIGURE 23. FAR FIELD SOUND LEVELS WITH AND WITHOUT TUNNEL FLOW (MICROPHONE 4, θ = 140°)

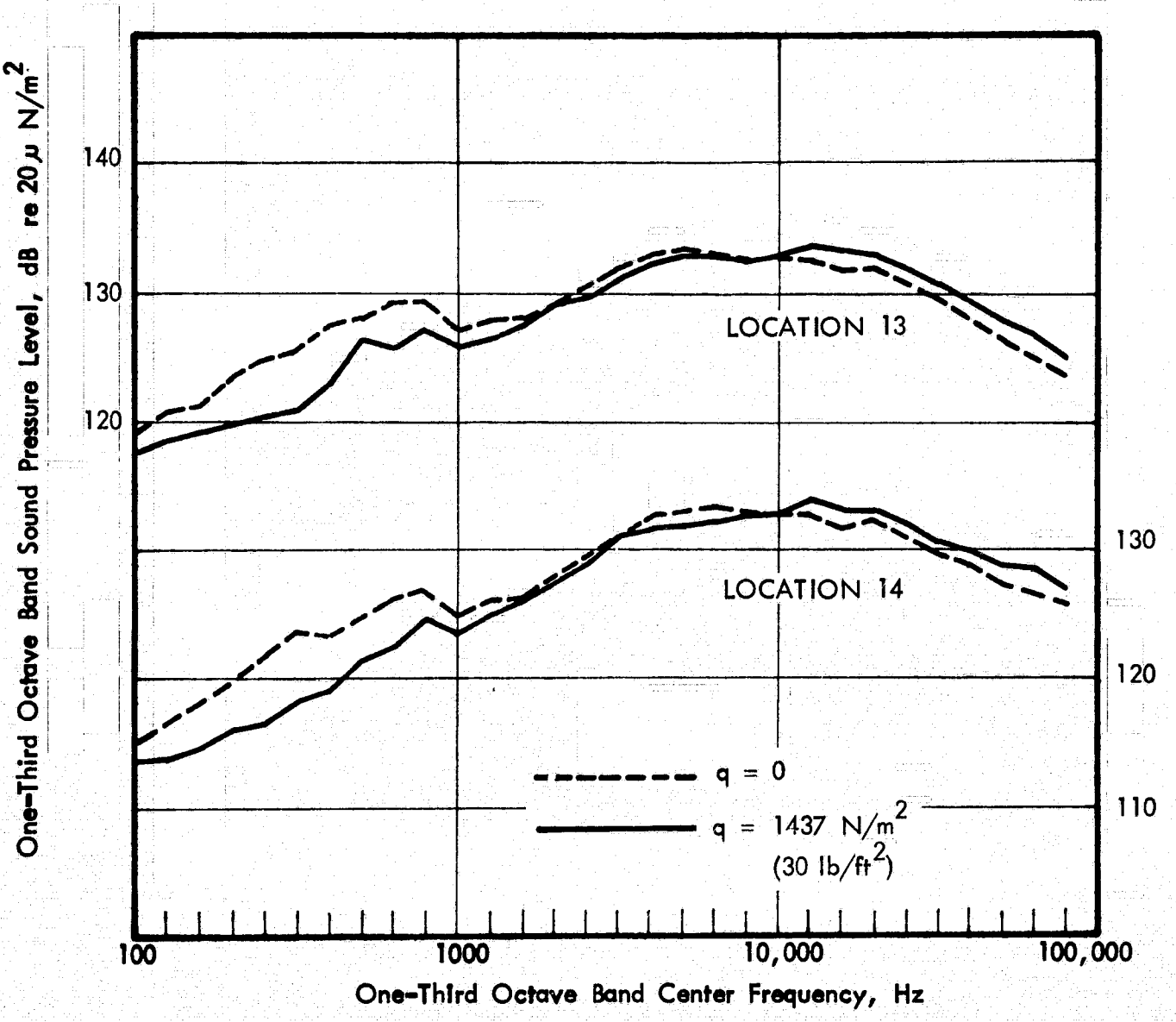

FIGURE 24. SURFACE PRESSURE SPECTRA NEAR FLAP TRAILING EDGE, WITH AND WITHOUT TUNNEL FLOW (P.R. = 2.09)

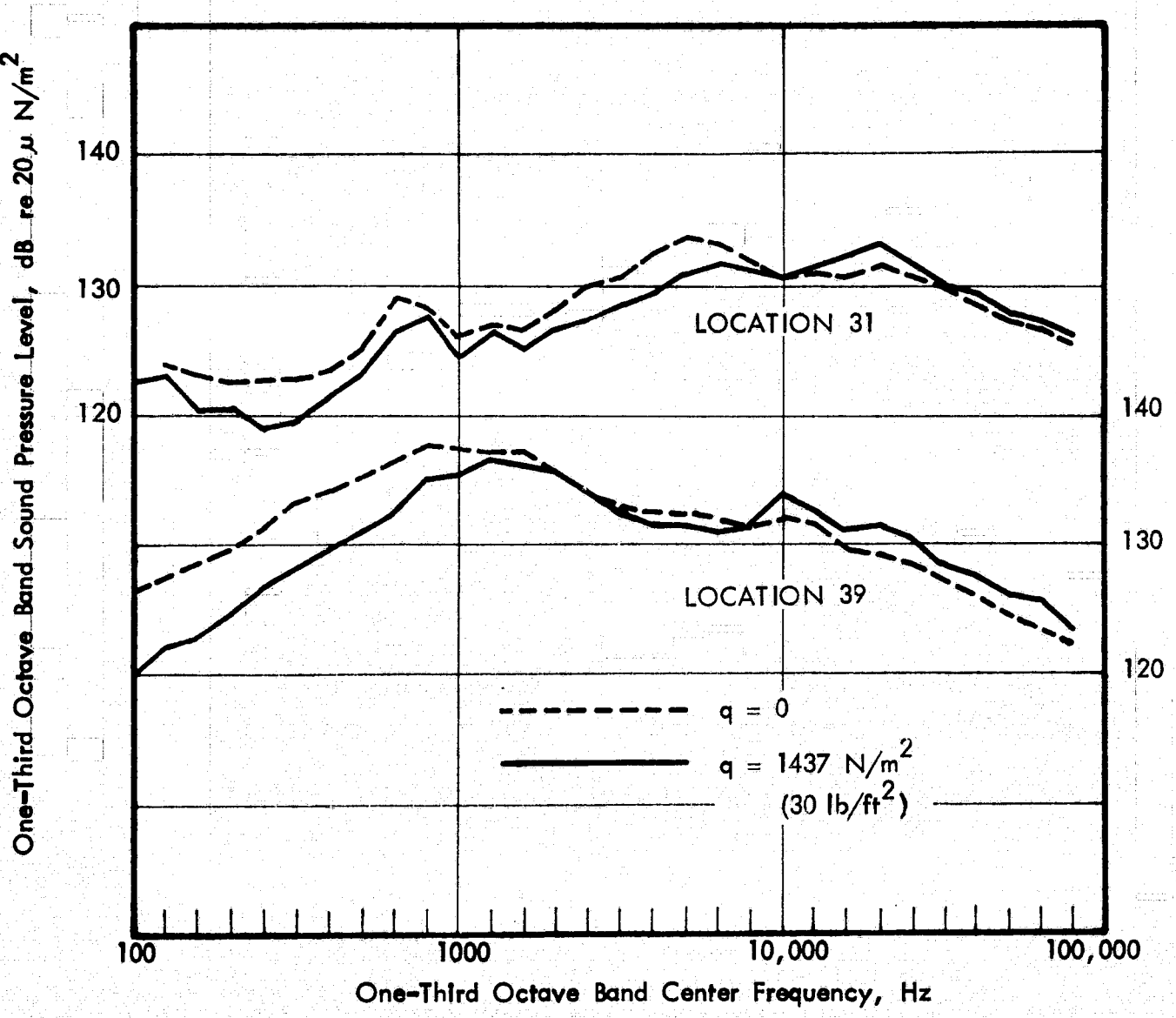

FIGURE 25. SURFACE PRESSURE SPECTRA ON SHROUD, WITH AND WITHOUT TUNNEL FLOW (P.R. = 2.09)

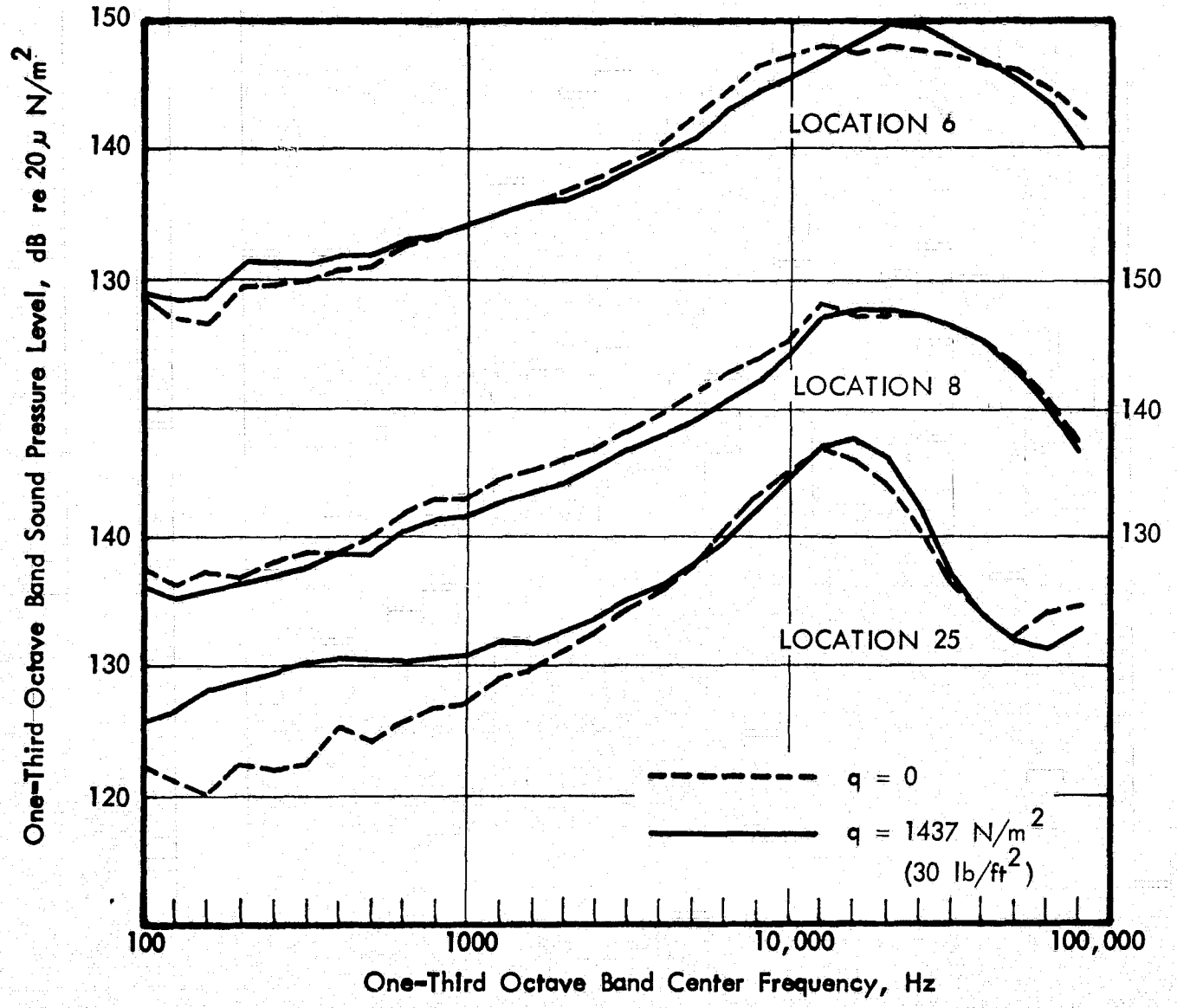

FIGURE 26. SURFACE PRESSURE SPECTRA AT FLAP LEADING EDGE, WITH AND WITHOUT TUNNEL FLOW (P.R. = 2.09)

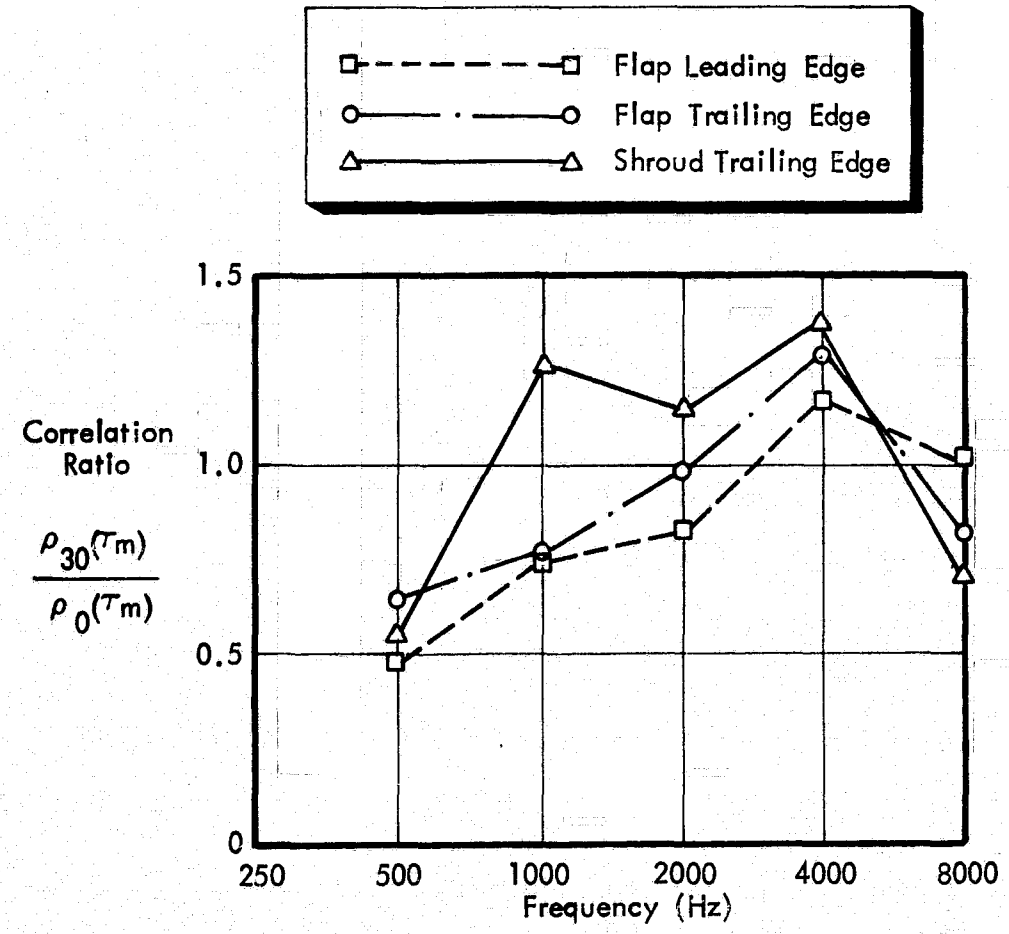

FIGURE 27. EFFECT OF TUNNEL FLOW ON SURFACE-TO FAR-FIELD PRESSURE CORRELATION COEFFICIENT

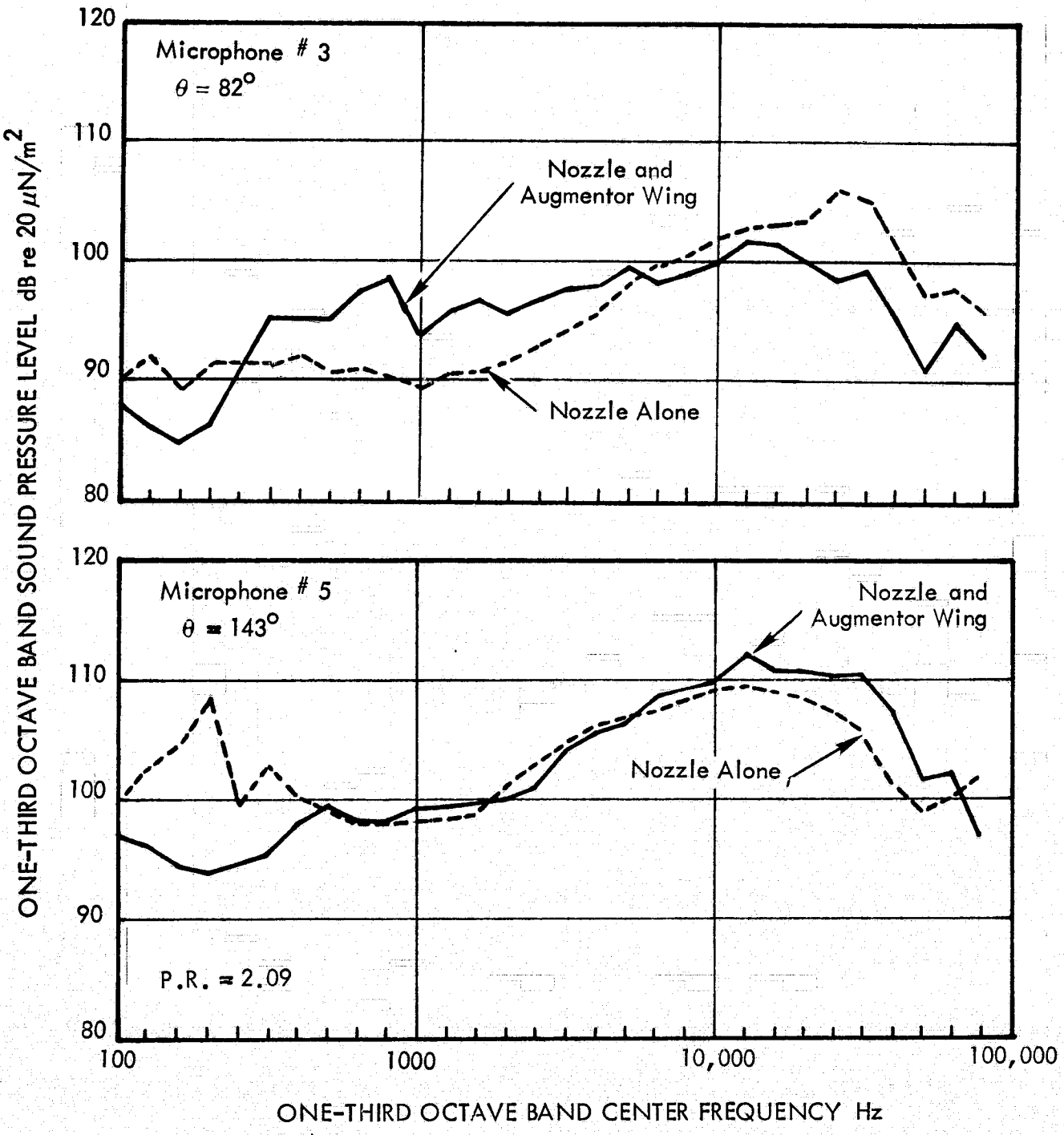

FIGURE 28. FAR FIELD ACOUSTIC SPECTRA FOR MODEL NOZZLE WITH AND WITHOUT AUGMENTOR WING.

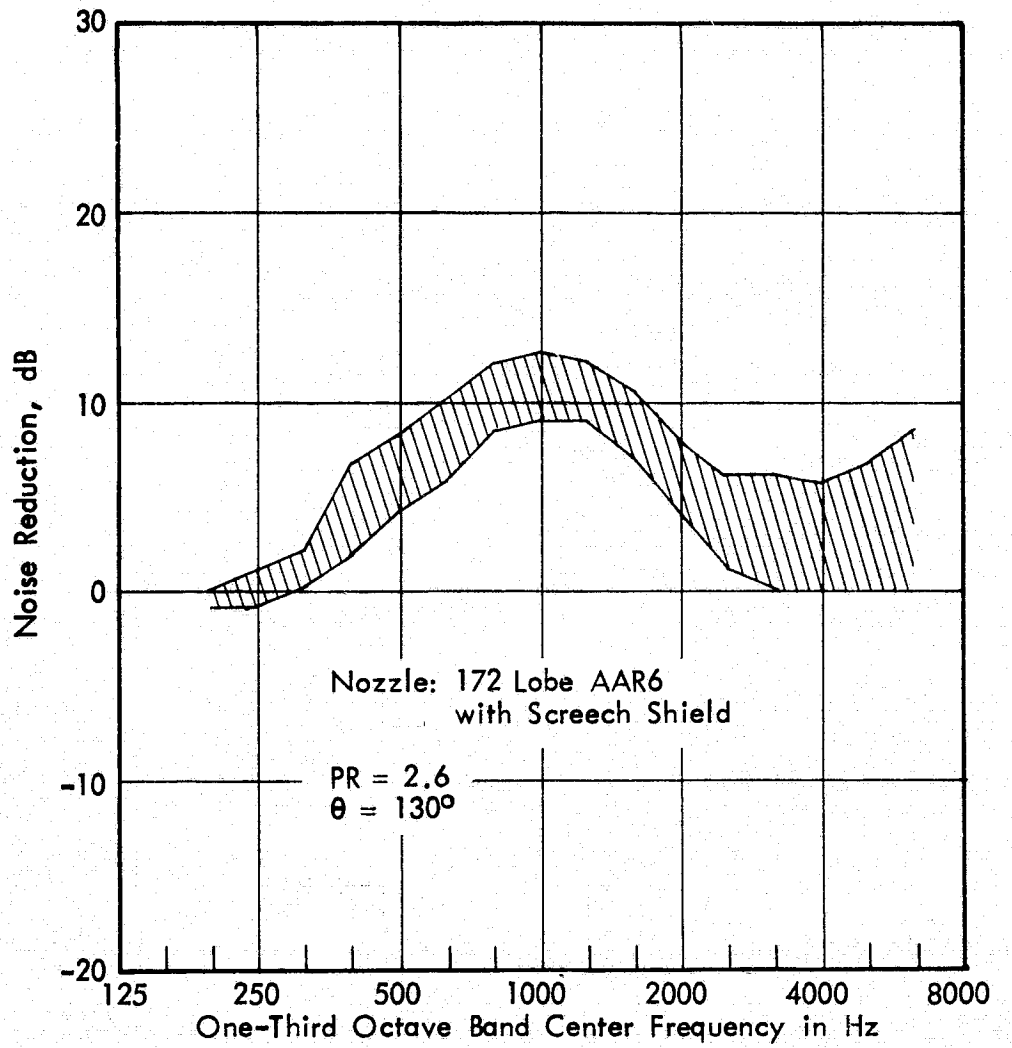

FIGURE 29. NOISE REDUCTION ACHIEVED BY LINING MODEL SCALE AUGMENTOR FLAP AND SHROUD (Ref. 1)